

Tsunami Hazard Assessment of Bainbridge Island, Washington Project Report

Draft of November 30, 2018

Vasily V. Titov, Diego Arcas, Christopher W. Moore
Pacific Marine Environment Laboratory, NOAA, Seattle

Randall J. LeVeque, Loyce M. Adams, Frank I. González
University of Washington

Study funded by Washington State Emergency Management Division

http://depts.washington.edu/ptha/WA_EMD_Bainbridge/

Contents

1	Introduction	4
2	Study area	4
3	Earthquake Sources	4
3.1	Cascadia megathrust event CSZ-L1	5
3.2	Seattle Fault event SF-L	8
4	Topography and Bathymetry	8
4.1	1/3 Arc-second DEMs	8
5	Modeling uncertainties and limitations	8
5.1	Tide stage and sea level rise	8
5.2	Subsidence and uplift	8
5.3	Structures	9
5.4	Bottom friction	9
5.5	Tsunami modification of bathymetry and topography	9
6	The MOST model	9
7	The GeoClaw model	10
8	Results and model comparison	10
8.1	Maximum depth and speed maps	10
8.2	Gauge comparisons	14
8.2.1	Gauge comparisons for SF-L	15
8.2.2	Gauge comparisons for L1	19
	Appendices	22
A	Additional comparisons of results for SF-L	22
A.1	Zoomed views and transect plots	22
A.1.1	Seattle Fault SF-L, Eagle Harbor	23
A.1.2	Seattle Fault SF-L, Murden Cove	26
A.1.3	Seattle Fault SF-L, Agate Pass	28
A.1.4	Seattle Fault SF-L, Point White	30
B	Additional comparisons of results for CSZ L1	32
B.1	Zoomed views and transect plots	32
B.1.1	CSZ L1, Eagle Harbor	33
B.1.2	CSZ L1, Murden Cove	36

B.1.3 CSZ L1, Agate Pass	38
B.1.4 CSZ L1, Point White	40
C GeoClaw Data format	42
Acknowledgments	43
References	43

1 Introduction

This report documents the results of a study supported by the Washington State Emergency Management Division of the tsunami hazard along the coast of Bainbridge Island, WA. One earthquake source from the Seattle Fault and one from the Cascadia Subduction Zone were considered. Results include inundation depths and times of arrival that will be useful to coastal communities, as well as tsunami current speeds and momentum flux.

In this collaborative project between the UW Tsunami Modeling group and the NOAA Center for Tsunami Research at PMEL, a comparison has also been performed between the results obtained by the two groups using two different computer codes:

- The UW group used GeoClaw Version 5.5.0 [4].
- The PMEL group used MOST GPU v2.6.3.

Both software packages solve the two-dimensional shallow water equations over variable topography and bathymetry with the addition of bottom friction in the form of a Manning coefficient. Identical sea floor deformations were used by the two groups to initiate the tsunami. The same finest grid resolution (1/3 arcsecond resolution in both longitude and latitude) was also used around the study region described in Section 2.

In principle the two codes should produce very similar results. Exact agreement is not expected because there are numerous differences in the numerical methods that are implemented to discretize the shallow water equations, in the algorithms used to handle wetting and drying at margins of the flow, in the coarser level grids that surround the study region, and in numerous other details. These differences are described in more detail in Sections 7 and 6.

The conclusion of our comparison is that the two codes do give very similar results, well within the expected variance in view of the model differences. Some sample results and comparisons are shown in Section 8 and the Appendices. This is an important validation exercise for each code, and is particularly important in view of the fact that the PMEL and UW groups are, in other on-going projects, modeling different portions of the Washington State coastline in support of the new generation of hazard maps being produced by DNR. This study suggests that the results produced by the two groups should be similar also in other regions, and hence seamless integration of the modeling results into hazard products should be possible with little concern that different results would be obtained by the other group.

2 Study area

Figure 1 shows the study area surrounding Bainbridge Island. The rectangle labelled “A grid” shows the region where a 1/3” computational grid is used in MOST, and where refinement to this level is forced in GeoClaw. Outside of this region coarser computational grids are used. This plot also indicates four regions where comparisons between MOST and GeoClaw are presented in Appendices A and B.

3 Earthquake Sources

Two earthquake sources were considered for this study: a Cascadia Subduction Zone (CSZ) megathrust event with moment magnitude Mw 9.0 (denoted CSZ-L1), and a potential Seattle Fault rupture denoted SF-L.

The CSZ-L1 event creates very large waves along the outer coast and a substantial wave that propagates into the Strait of Juan de Fuca (SJdF) and into Puget Sound, affecting parts of Bainbridge Island, starting about 2 hours after the earthquake. No subsidence or uplift is produced by CSZ-L1 in Puget Sound. There is little significant flooding on the island from this event, but some very strong currents are generated, particularly in Agate Pass at the north end of the island and around Point White in the south; see Figure 4.

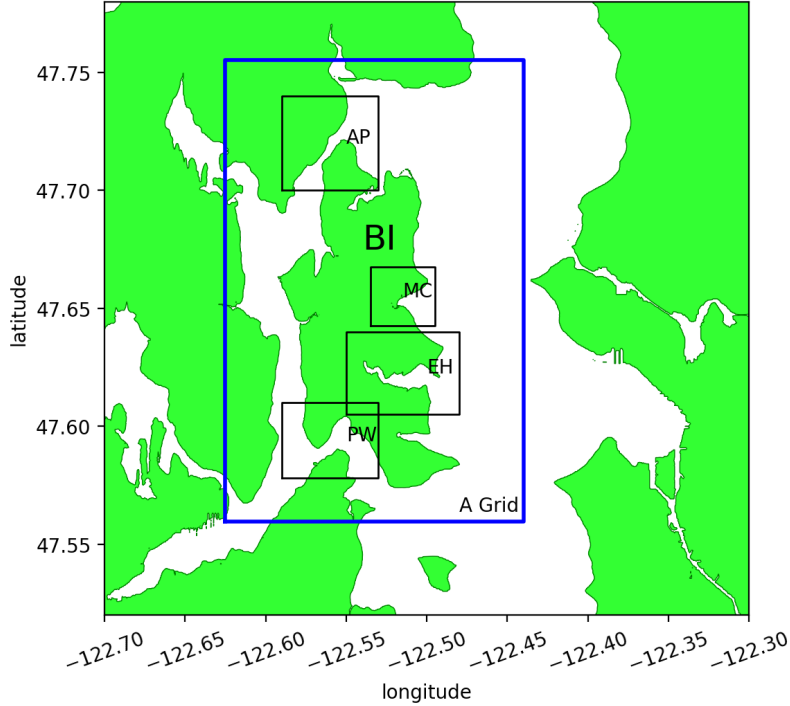


Figure 1: Bainbridge Island (BI), showing also the A grid region where a 1/3” computational grid is used and four regions where comparisons between MOST and GeoClaw are presented in Appendices A and B. **AP:** Agate Pass, **MC:** Murden Cove, **EH:** Eagle Harbor, and **PW:** Point White.

The Seattle Fault cuts across Puget Sound (through Seattle and Bainbridge Island) and can create a tsunami that affects the island immediately. The northern portion of the island subsides, increasing the level of flooding in Eagle Harbor and other coastal regions to the north. The southern portion of the island is uplifted and very little inundation is observed in these regions. However, very strong currents are observed in many locations all around the island; see Figure 3.

These two earthquake sources are described in more detail in the sections below. Other potential sources have not been considered in this study. In particular the smaller Seattle Fault event SF-S that has been used in some past tsunami studies in Puget Sound was found to have negligible impact and was not modeled in detail. Several other fault zones cross Puget Sound, but potential sources from these faults have not been considered.

3.1 Cascadia megathrust event CSZ-L1

The probability that an earthquake of magnitude 8 or greater will occur on the Cascadia Subduction Zone (CSZ) in the next 50 years has been estimated to be 10-14% (Petersen, et. al., 2002 [9]). The last such event occurred in 1700 (Satake, et al., 2003 [10]; Atwater, et al., 2005 [1]) and future events are expected to generate a destructive tsunami that will inundate Washington Pacific coast communities within tens of minutes after the earthquake main shock. Waves will travel through the Strait of Juan de Fuca and start arriving at Bainbridge Island roughly 2 hours and 15 minutes after the earthquake.

The potential CSZ event used in this study is the L1 scenerio developed by Witter, et al. (2013) [15]; crustal deformation for the region of interest is shown in Figure 2. The L1 source is one of 15 seismic scenarios used in a hazard assessment study of Bandon, OR, based on an analysis of data spanning 10,000 years. This scenario has been adopted by Washington State as the “maximum considered case” for many inundation modeling studies and subsequent evacuation map development; it is used because the standard engineering

planning horizon is 2500 years and Witter, et al. in 2013 [15] estimated that L1 has a mean recurrence period of approximately 3333 years, with the highest probability of occurrence of all events considered with magnitude greater than Mw9.

The original L1 source was developed for studies on the Oregon coast and was truncated at around 48N. An extension of this developed by PMEL has been used in this study. The seafloor deformation is shown in Figure 2.

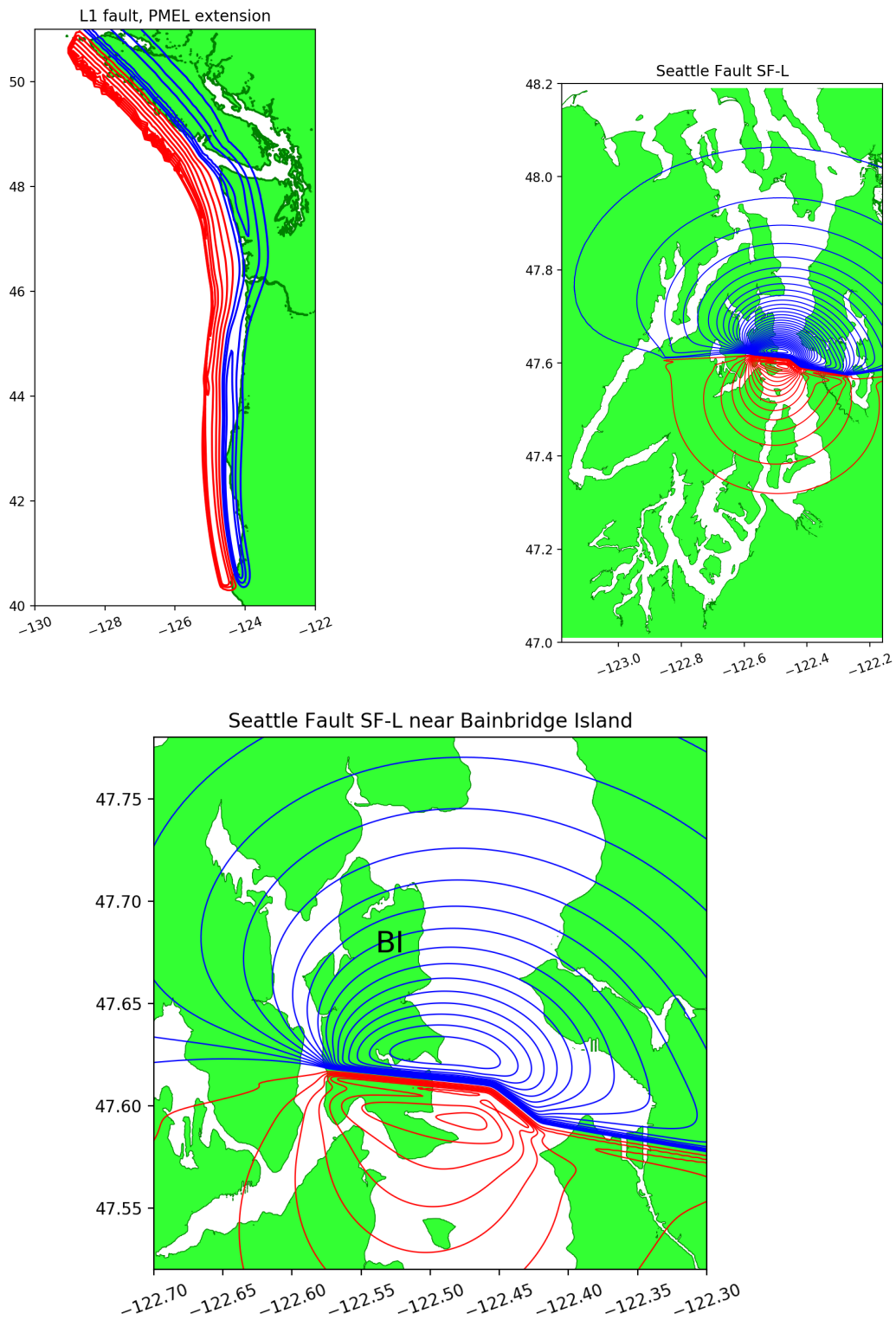


Figure 2: Top Left: Surface deformation of the L1 source, with maximum uplift 15.08 m and maximum subsidence -3.98 m. Red contours show uplift (2 meter interval), blue contours show subsidence (1 meter interval). Top Right: Surface deformation of the SF-L source, with maximum uplift 8.37 m and maximum subsidence -1.78 m. Red contours show uplift at levels 0.5, 1, 1.5, ... meters, blue contours show subsidence at levels -0.05 , -0.1 , ... meters. Bottom: Zoom of SF-L near Bainbridge Island (BI).

3.2 Seattle Fault event SF-L

Figure 2 shows contours of uplift and subsidence due to a hypothetical event on the Seattle fault that we denote by SF-L. Earlier tsunami hazard studies have referred to this as a Mw 7.3 event. However, when we tried to recreate the deformation field by applying the Okada model to the subfault parameters listed in [3], we determined that the magnitude should be Mw 7.54, as discussed in Appendix E of the Snohomish County report, [6]. Regardless of the proper magnitude, we are using the deformation file provided by PMEL that has been used for the previous tsunami hazard analyses of Everett [3].

Due to uncertainty about the magnitude, in [6] the SF-L notation was adopted for this larger Seattle Fault scenario, and we continue to use that here. The deformation was originally chosen to match observed uplift and subsidence at a few points around Puget Sound. Since the original specification of this deformation, many new observations have been made and improved models for the subfault geometry have also been produced. A new model for SF-L is now under development and in the future this could perhaps be used to update the results of the current study.

A smaller Seattle Fault scenario (SF-S) was also initially considered, but found to produce a very small tsunami.

4 Topography and Bathymetry

4.1 1/3 Arc-second DEMs

Output from the model was requested at grid points spaced 1/3" in longitude and 1/3" in latitude, with the points aligned with cell centers of the 1/3" DEM files that are available for the Puget Sound region. (Note that 1/3" in latitude is approximately 10.3 m. At this latitude, 1/3" in longitude is approximately 6.9 m).

Several topography DEMs provided by NCEI have been used in this study. The Puget Sound 1/3" DEM covers the Bainbridge Island region. In addition, the Port Townsend 1/3" DEM and the Strait of Juan de Fuca 1/3" DEM are used for coverage of the Strait, and etopo1 data (1 arcminute) is used for the portion of the Pacific Ocean needed for modeling the L1 source.

5 Modeling uncertainties and limitations

Both MOST and GeoClaw use the shallow water equations to model the tsunami, which is an approximation of the three-dimensional fluid dynamics, but one that has been found to be sufficiently accurate for inundation studies of this nature in previous studies, including validation and benchmarking workshops. However, it is only an approximation to the correct physics. A number of other assumptions or approximations are also made in both models, as summarized below.

5.1 Tide stage and sea level rise

The simulations were conducted with the background sea level set to MHW. This value is conservative, in the sense that the severity of inundation will generally increase with a higher background sea level. Larger tide levels do occasionally occur, but the assumption of MHW is standard practice in studies of this type. Potential sea level rise over the coming decades was not taken into account in this modeling.

5.2 Subsidence and uplift

The Seattle Fault cuts across Bainbridge Island, and so the SF-L event induces significant subsidence to the north and uplift to the south of the fault. This ground motion is taken into account in both tsunami

models, and it is the underwater vertical motion that generates the tsunami. For both events, the details of the motion depend on the hypothetical earthquake source used, and this is the biggest source of uncertainty in the model results since the next earthquake may be very different from the ones that have been modeled.

5.3 Structures

Buildings were not included in the simulations, the topographic DEMs provided for this study are “bare earth”. The presence of structures will alter tsunami flow patterns and generally impede inland flow. To some extent the lack of structures in the model is therefore a conservative feature, in that their inclusion would generally reduce inland penetration of the tsunami wave. However, as in the case of the friction coefficient, impeding the flow can also result in deeper flow in some areas. It can also lead to higher fluid velocities, particularly in regions where the flow is channelized, such as when flowing up streets that are bounded by buildings.

5.4 Bottom friction

Mannings coefficient of friction was set to 0.025 in GeoClaw and to 0.03 in MOST, standard values used in tsunami modeling that corresponds to gravelly earth. Slightly different values were used for historical reasons based on the requirements of past modeling studies. A choice in this range is conservative in some sense, because the presence of trees, structures and vegetation would justify the use of a larger value, which might tend to reduce the inland flow. On the other hand, larger friction values can lead to deeper flow in some areas, since the water may pile up more as it advances more slowly across the topography.

5.5 Tsunami modification of bathymetry and topography

Severe scouring and deposition are known to occur during a tsunami, undermining structures and altering the flow pattern of the tsunami itself. Again, this movement of material requires an expenditure of tsunami energy that tends to reduce the inland extent of inundation. On the other hand, if natural berms or ridges along the coastline (or man-made levies or dikes) are eroded by the tsunami, then some areas can experience much more extensive flooding. There is no erosion or deposition included in the simulations presented here.

6 The MOST model

MOST (Method Of Splitting Tsunami) is a suite of numerical simulation codes to simulate three processes of tsunami evolution: generation by earthquake, transoceanic propagation, and inundation onto dry land. The model uses finite difference numerical scheme to solve the nonlinear shallow water equation [12, 13]. The MOST model has been extensively tested against a number of laboratory experiments and benchmarks [11, 12, 13, 14] as part of the NSF-funded tsunami modeling benchmark workshops. Additional testing have been conducted for MOST as part of the operational testing and evaluation for implementation into NOAA Tsunami Warning System operational tsunami forecast as part Short-term Inundation Forecast for Tsunamis (SIFT) capability of the Tsunami Warning Centers [13]. The MOST has been operational forecast model at NOAAs TWCs since 2012.

MOST uses a set of three nested grids, referred to as A, B, and C grids, each of which becomes successively finer in resolution as they telescope into the community of interest. A separate propagation model was used to compute the propagation from the L1 source offshore Cascadia and tsunami propagation into the Strait of Juan de Fuca and further into the Puget Sound. The propagation model is run with 34 arc-second resolution. The offshore area is covered by the largest and lower-resolution A grid with the resolution of 30 arc-seconds, grid B of 2 arc-seconds. The highest resolution C grids has the same resolution (1/3 arc-second) and extent for both models.

The finite difference model in MOST used pointwise topography values at grid points, taken directly from the topography DEMs.

7 The GeoClaw model

The GeoClaw model is part of Clawpack [4], and has undergone extensive verification and validation (e.g. [2, 7]), and has been accepted as a validated model by the U.S. National Tsunami Hazard Mitigation Program (NTHMP) after conducting multiple benchmark tests as part of an NTHMP benchmarking workshop [5].

GeoClaw uses finite volume methods with adaptive mesh refinement. The finest grid resolution near regions of interest was set to the desired resolution of $1/3''$ by $1/3''$. The specified topography DEM files is viewed as providing pointwise values. From these values a piecewise bilinear interpolating function is constructed in two dimensions and this function is integrated over the finite volume cells actually used in the computation. The finest grid was aligned so that cell centers agree with DEM points, but the actual topography value used by GeoClaw in each cell is an average of the piecewise bilinear function in this cell and will not agree exactly with the DEM value at the cell center. Consequently the topography value used in a GeoClaw grid cell is not identical to the value used at the corresponding grid point in MOST.

Away from the study region, coarser computational grids are used. GeoClaw uses Adaptive Mesh Refinement (AMR) to allow the grid resolution to vary during the course of the computation in order to introduce finer grids only as a wave approaches a region. For the L1 simulations the coarsest grids had a resolution of $6'$, although the region waves have reached had a resolution of $30''$ or better in the Pacific, $6''$ in the Strait of Juan de Fuca and Puget Sound, and $2''$ in an area roughly corresponding to the B-grid of the MOST model. For the SF-L simulations, a smaller computational domain was used that covered only the Puget Sound with a $30''$ coarse grid, allowing refinement to $6''$ as waves arrive, and up to $1''$ in an area roughly corresponding to the B-grid of the MOST model.

8 Results and model comparison

In this section some sample results are shown. We have not attempted to produce high quality graphics of the results, since Washington State DNR is producing the maps that will be published elsewhere. Our goal is to illustrate the results obtained and the level of agreement between the results obtained with the two different codes MOST and GeoClaw.

8.1 Maximum depth and speed maps

The primary products of this work that will go into hazard maps produced by DNR are the maximum flooding depth over the entire tsunami event, at each point on shore, and the maximum flow speed, both at points on shore and in the harbors and water ways surrounding the island. Hence a comparison of these maxima is of primary interest. Figures 3 and 4 show the results for the SF-L and CSZ L1 event respectively.

In addition, time series of the depth (or water surface) and speed at selected synthetic gauge locations provide a way to compare the time evolution of the different simulations. These are shown in Section 8.2.

In the appendices we present more detailed view of these comparisons over a few regions of particular interest, along with some selected transects to make it easier to compare and judge the results.

In general we have found excellent agreement between results produced by the two different codes. As we expected, the water depth generally agrees better than the speeds, both in terms of maximum values and in the time series at gauge locations. It is well known that current speeds vary much more dramatically in both space and time than fluid depth [8]. For example, vortices generated at a harbor entrance produce concentrated regions of very high velocity even though the surface elevation may differ only slightly from the surrounding water. The path that a vortex takes away from the point of generation can be very sensitive to

small changes in the flow, and may result in very different maximum speed or time series at any given point if the input data is changed slightly, or if the numerical method used to compute the flow is changed. As a result of this, one can identify several points where GeoClaw and MOST produce quite different speeds. In general, however, the overall patterns of maximum speed in a given region are very similar between the two codes.

We also found better agreement of gauge time series for the SF-L simulations than for L1. For the Cascadia Subduction Zone L1 simulations, the tsunami is generated in the ocean and travels through the Strait of Juan de Fuca and Puget Sound to reach Bainbridge Island. The first (and typically largest) waves observed at the gauges agree quite well, but later waves show more deviation. These later waves arise from sloshing in the Sound and may require a finer resolution over the entire Sound than was used in this study in order to capture them accurately.

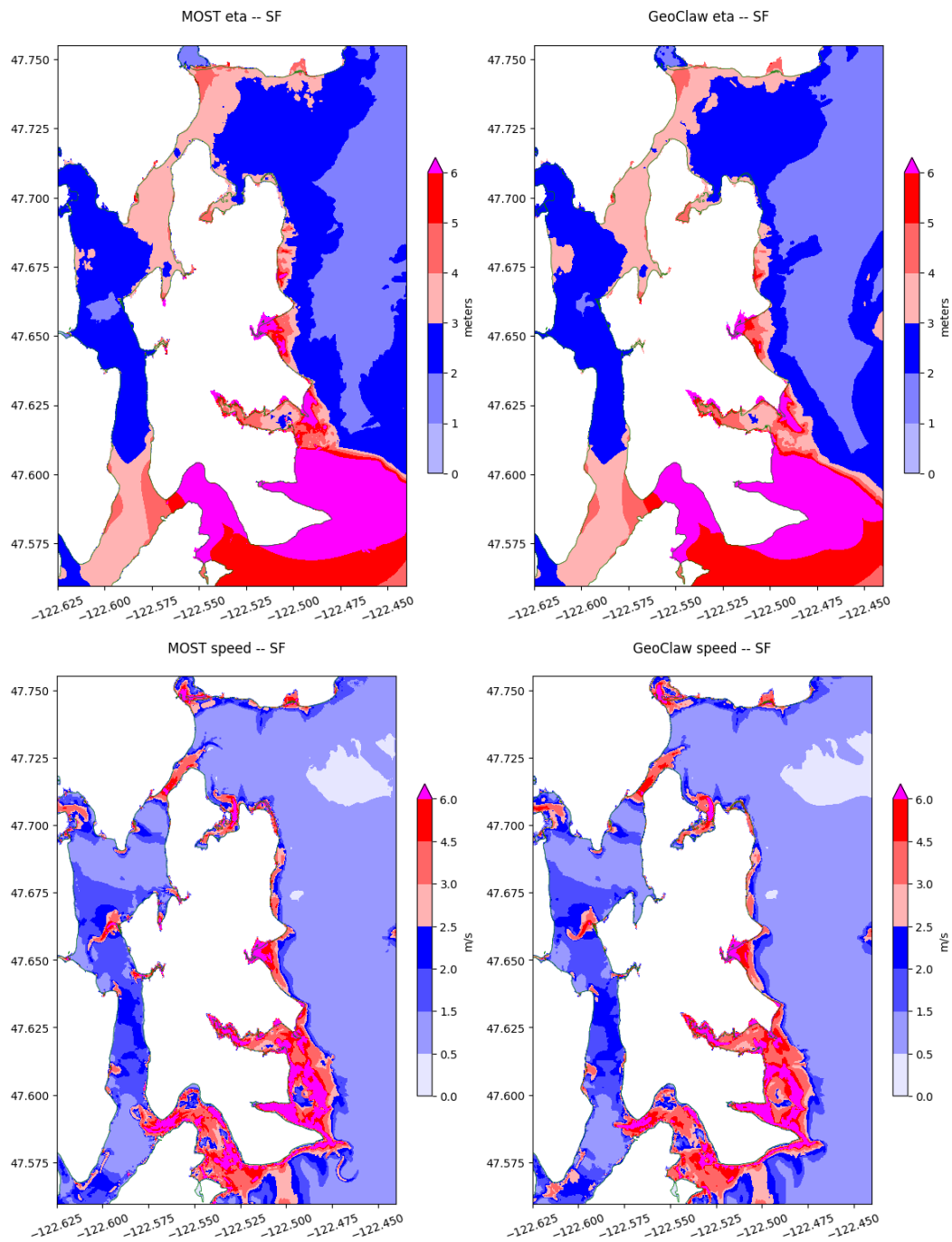


Figure 3: Comparison of results for the SF-L event. Maximum surface elevation (top) and flow speed (bottom) for MOST (left) and GeoClaw (right) simulations.

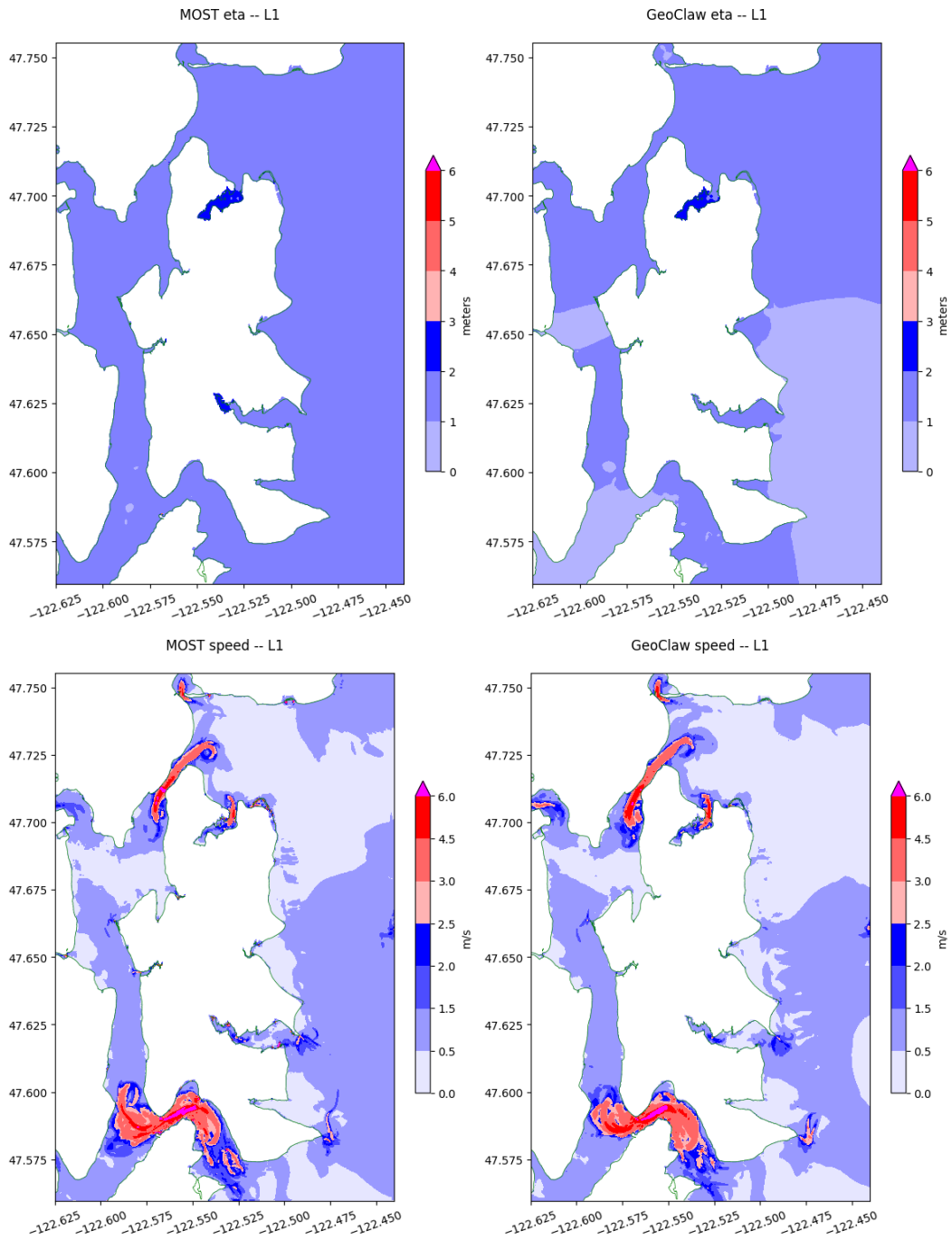


Figure 4: Comparison of results for the CSZ L1 event. Maximum surface elevation (top) and flow speed (bottom) for MOST (left) and GeoClaw (right) simulations.

8.2 Gauge comparisons

Time series of the depth (or water surface) and speed at selected synthetic gauge locations provide a way to compare the time evolution of the different simulations.

The following plots show time series at several synthetic tide gauge locations around Bainbridge Island, with locations listed in Table 1 and indicated in Figure 5.

Number	Longitude	Latitude	Location
12	-122.5660484	47.7123548	WA 305 Bridge (Agate Pass)
13	-122.5663415	47.5885810	Point White
14	-122.5088982	47.6222184	Winslow ferry terminal (Eagle Harbor)
15	-122.5307267	47.6252105	Strawberry Plant Park (Eagle Harbor)
16	-122.5181688	47.6519844	Murden Cove
17	-122.5124237	47.7091317	Hedley Spit
18	-122.5279064	47.7031305	Port Madison

Table 1: Synthetic gauge locations specified by DNR.

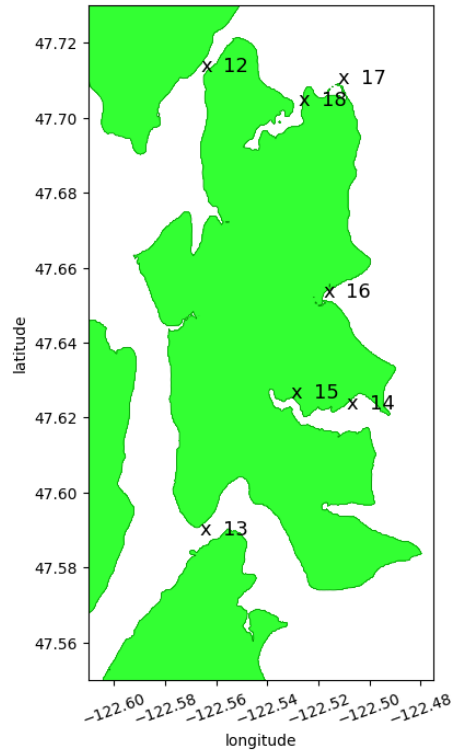


Figure 5: The location of synthetic gauges around Bainbridge Island.

8.2.1 Gauge comparisons for SF-L

Only the surface elevation is shown in these plots. The simulations were run for three hours of simulated time, but the largest waves arrive at most Bainbridge Island locations within the first hour, so for each gauge we also show an expanded view of the first 60 minutes in which it is easier to compare the results.

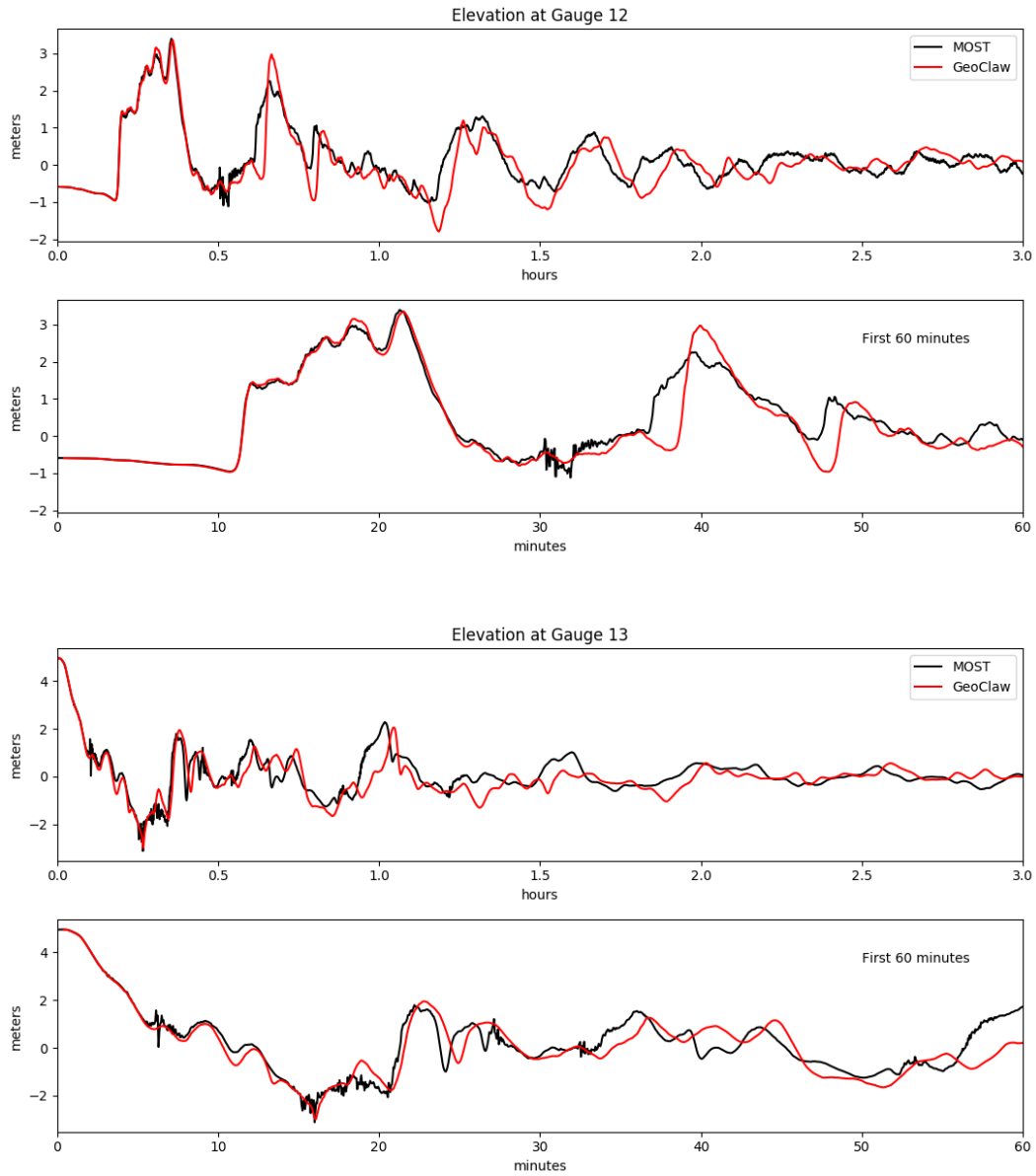


Figure 6: Comparison of MOST and GeoClaw gauge results for SF-L, over 3 hours and zoomed in on the first 60 minutes. Gauges 12 (WA 305 bridge, Agate Pass) and 13 (Point White).

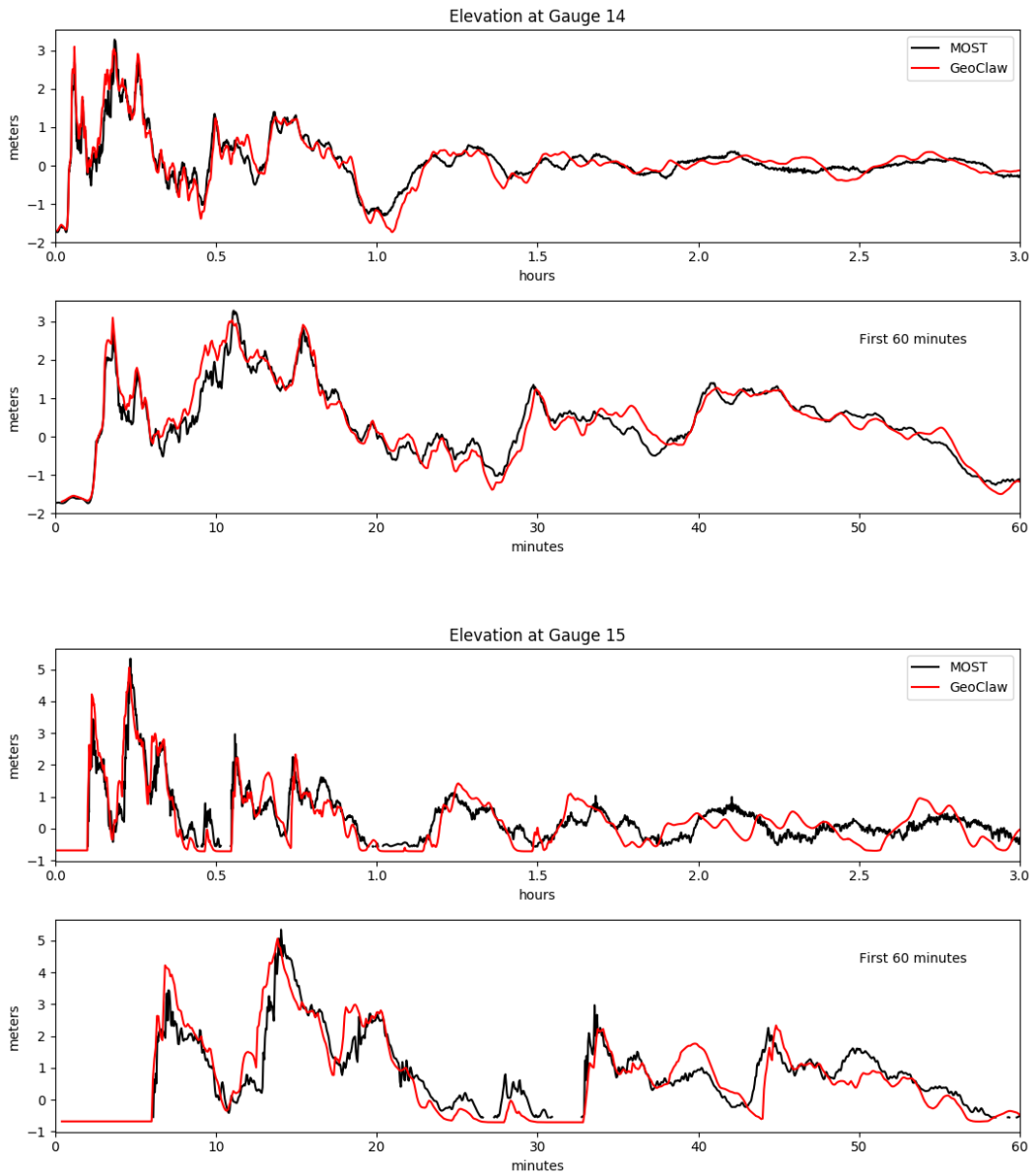


Figure 7: Comparison of MOST and GeoClaw gauge results for SF-L, over 3 hours and zoomed in on the first 60 minutes. Gauges 14 (Winslow Ferry Terminal) and 15 (Strawberry Park).

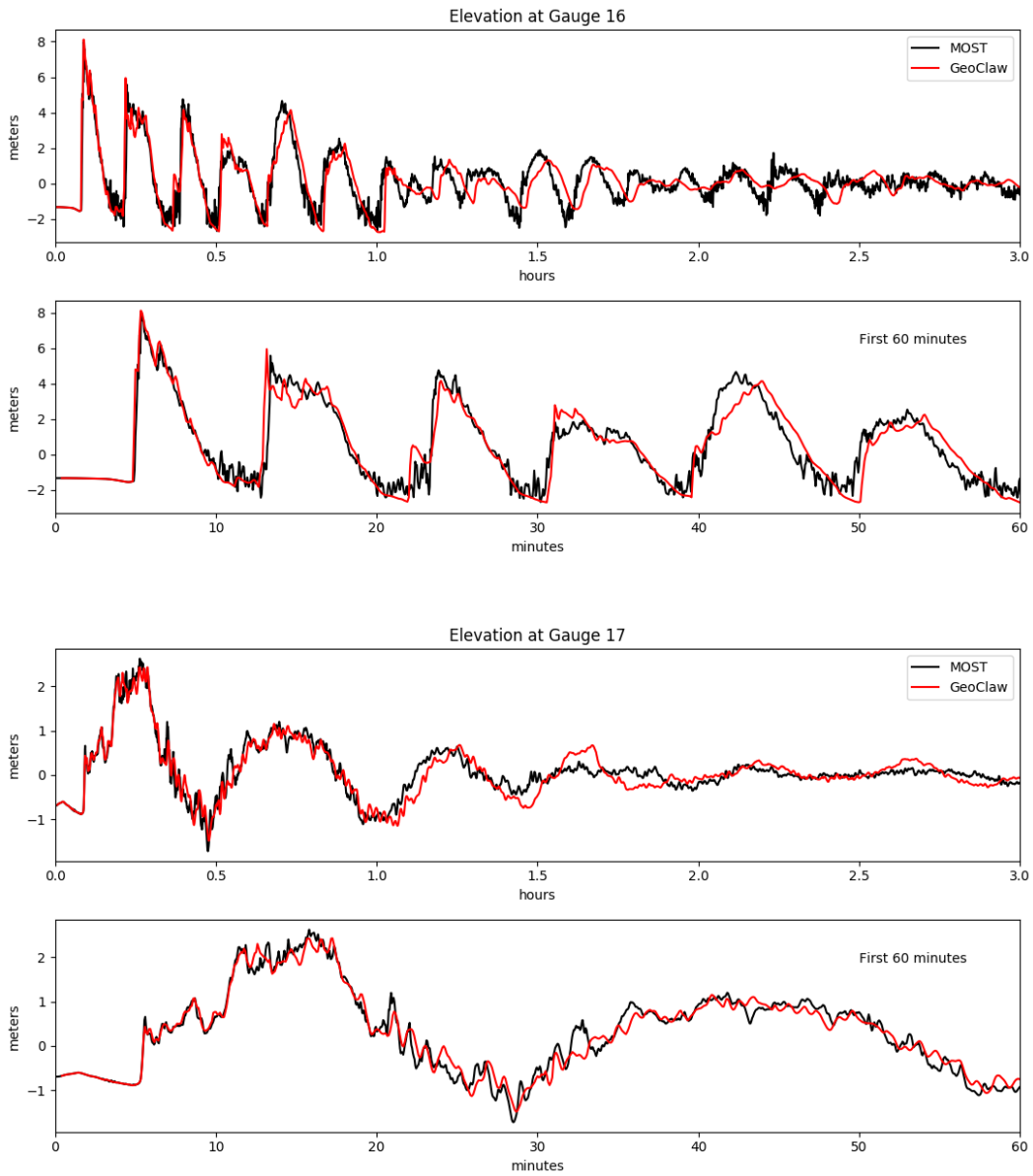


Figure 8: Comparison of MOST and GeoClaw gauge results for SF-L, over 3 hours and zoomed in on the first 60 minutes. Gauges 16 (Murden Cove) and 17 (Hedley Spit).

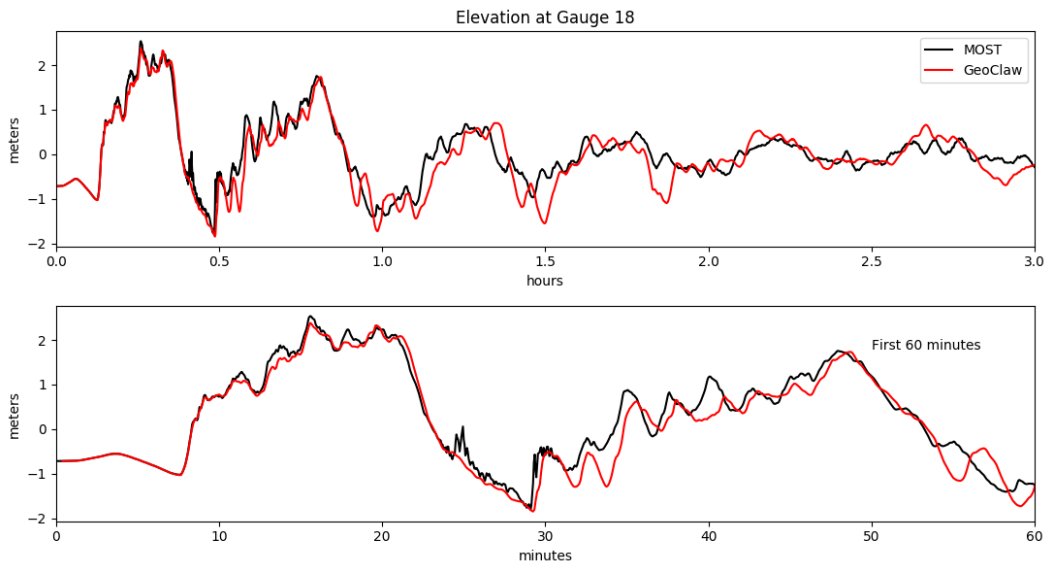


Figure 9: Comparison of MOST and GeoClaw gauge results for SF-L, over 3 hours and zoomed in on the first 60 minutes. Gauge 18 (Port Madison).

8.2.2 Gauge comparisons for L1

The following plots show time series at several synthetic tide gauge locations around Bainbridge Island, with locations listed in Table 1 and indicated in Figure 5. Only the surface elevation is shown in these plots. The positive wave of the tsunami from the L1 source does not arrive at Bainbridge Island until more than 2 hours after the earthquake, although a draw down of water is seen starting about an hour after the event. This is due to the fact that there is subsidence extending east of the trench into the Strait of Juan de Fuca, giving a leading negative wave propagating into the Puget Sound. The uplift occurs west of the trench and so the positive wave arrives later.

In the GeoClaw simulations the tide gauges were not turned on until 1.5 hours after the earthquake since the finest levels of grid refinement around Bainbridge are introduced only at this time.

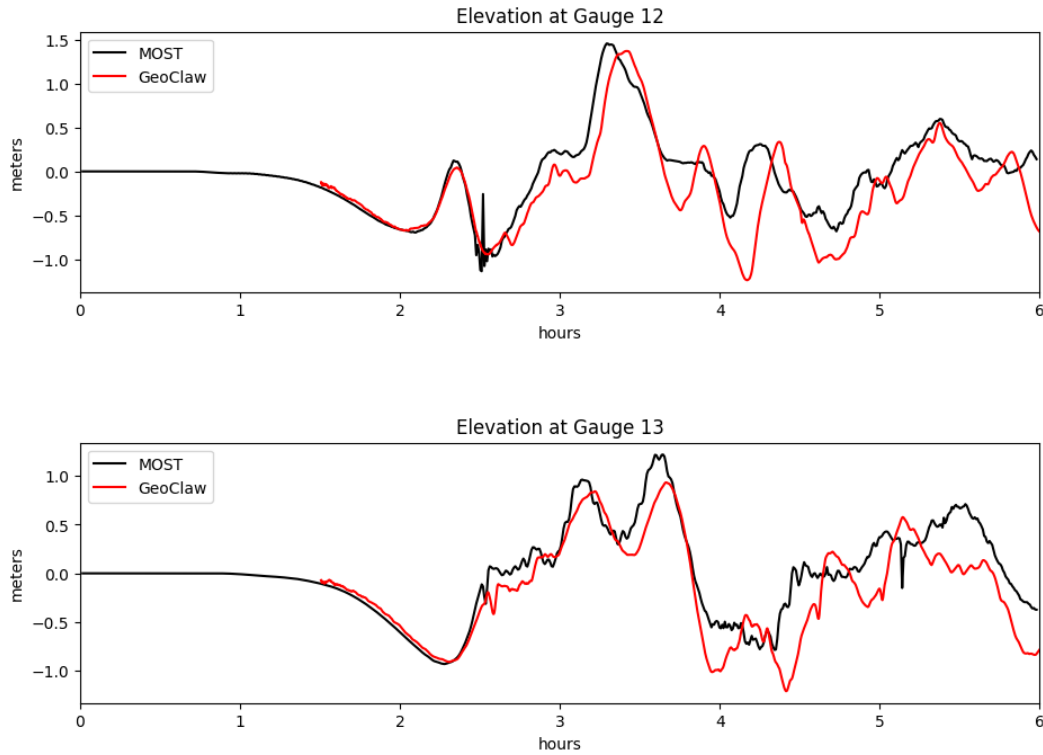


Figure 10: Comparison of MOST and GeoClaw gauge results for L1 over 6 hours. Gauges 12 (WA 305 bridge, Agate Pass) and 13 (Point White).

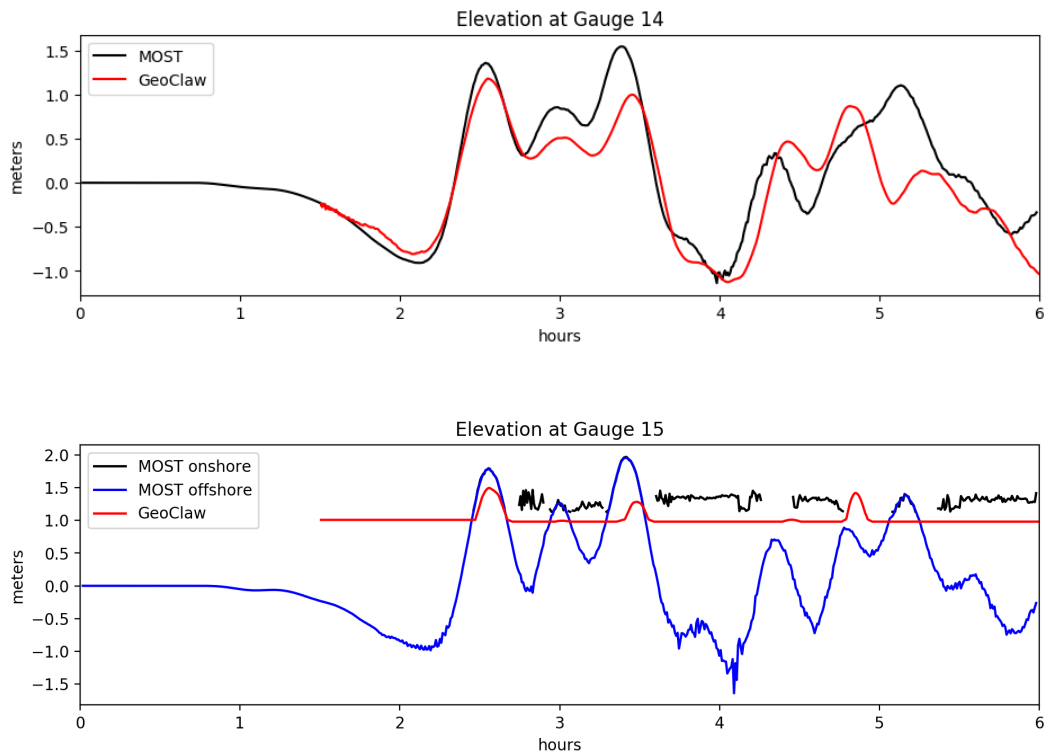


Figure 11: Comparison of MOST and GeoClaw gauge results for L1 over 6 hours. Gauges 14 (Winslow Ferry Terminal) and 15 (Strawberry Park). Note that Gauge 15 is onshore and MOST results are plotted both for this location and for an offset location that is offshore.

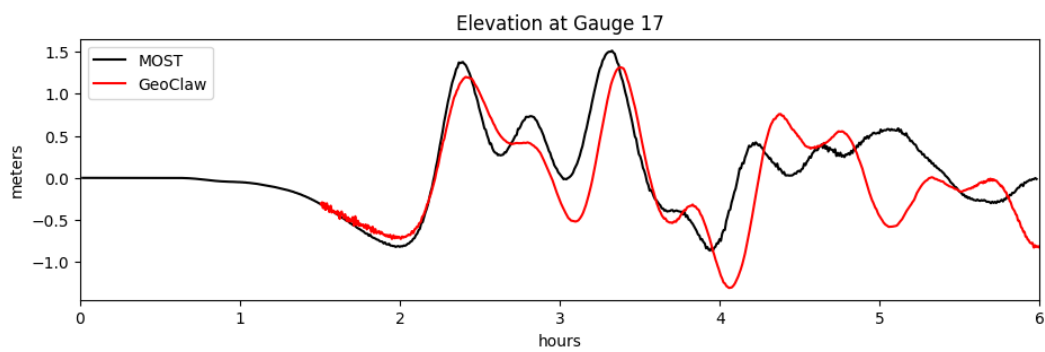
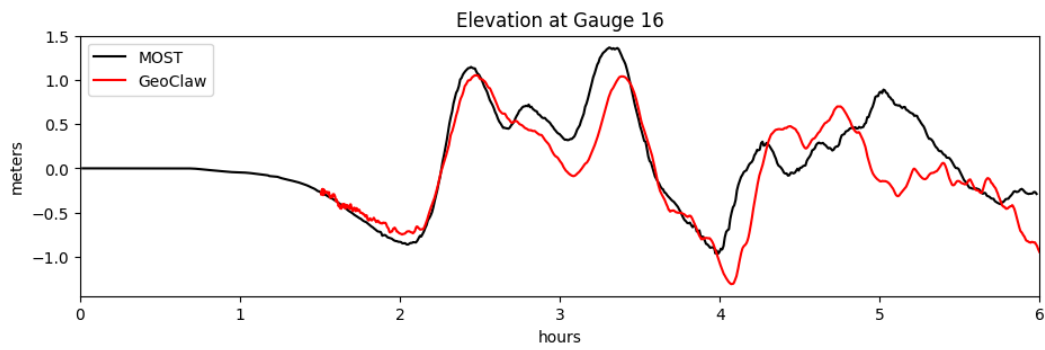


Figure 12: Comparison of MOST and GeoClaw gauge results for L1 over 6 hours. Gauges 16 (Murden Cove) and 17 (Hedley Spit).

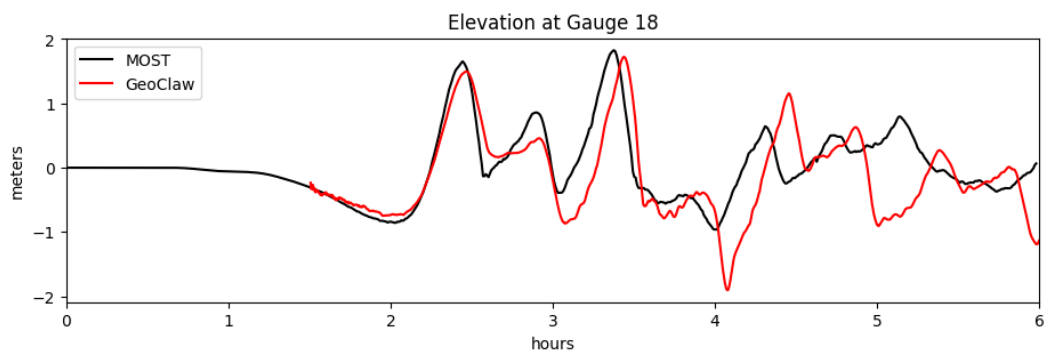


Figure 13: Comparison of MOST and GeoClaw gauge results for L1 over 6 hours. Gauge 18 (Port Madison).

Appendices

A Additional comparisons of results for SF-L

This appendix contains additional plots comparing the results obtained with MOST and those obtained with GeoClaw, for the Seattle Fault event SF-L. Section A.1 shows zoomed in views of the plots from Figure 3 along with cross sections of the solution on a few transects.

A.1 Zoomed views and transect plots

The plots in the next sections first show a zoomed view of one portion of Bainbridge Island, with several transect locations indicated.

Then the following plots show vertical slices along these transects. The top plot in each pair shows the maximum surface elevation of the flow over the full simulation time. (black curve is MOST, red is GeoClaw). These plots also show the vertical slice of the final topography and subsurface, after the earthquake, relative to the vertical scale on which 0 is always MHW. The green/brown coloring of the subsurface is used to indicate what portion of the subsurface initially had elevation greater than 0 (green), or below 0 (brown) before the earthquake. Before the earthquake, the interface between green and brown would have been at elevation 0, so displacement of the interface up or down indicates uplift or subsidence, respectively. The blue in some plots shows the water level long after the earthquake, after the tsunami has dissipated. The final water level is still 0 at MHW, and note that in regions of subsidence some green regions of the topography are now underwater, while in regions of uplift some of the brown seafloor is now exposed at MHW.

All of the transects shown below are regions of subsidence except for Point White, at the southwest corner of Bainbridge Island. In this location of uplift, note that the maximum surface elevation agrees with the original shoreline location, meeting the topography at the brown/green interface. This indicates that the maximum elevation occurred immediately after the earthquake. The water rose with the land initially, and then flowed away towards the subsided regions. All of the other transects, in regions of subsidence, generally show that the maximum was above both the initially subsided sea surface and the eventual new sea surface, and has captured the maximum of the transient tsunami waves.

The regions that are gray in these plots are regions where transect data of the topography was not available because the topography is above 40 m, due to the manner in which fgmax points were defined in GeoClaw. There was never any inundation at these points.

The bottom plot in each pair of transect slices shows the maximum flow speed over the same range of latitudes as in the top plot. In general the speeds are less smooth and do not agree between MOST and GeoClaw quite as well as the elevations. This is expected due to the extreme sensitivity of the flow speeds.

A.1.1 Seattle Fault SF-L, Eagle Harbor

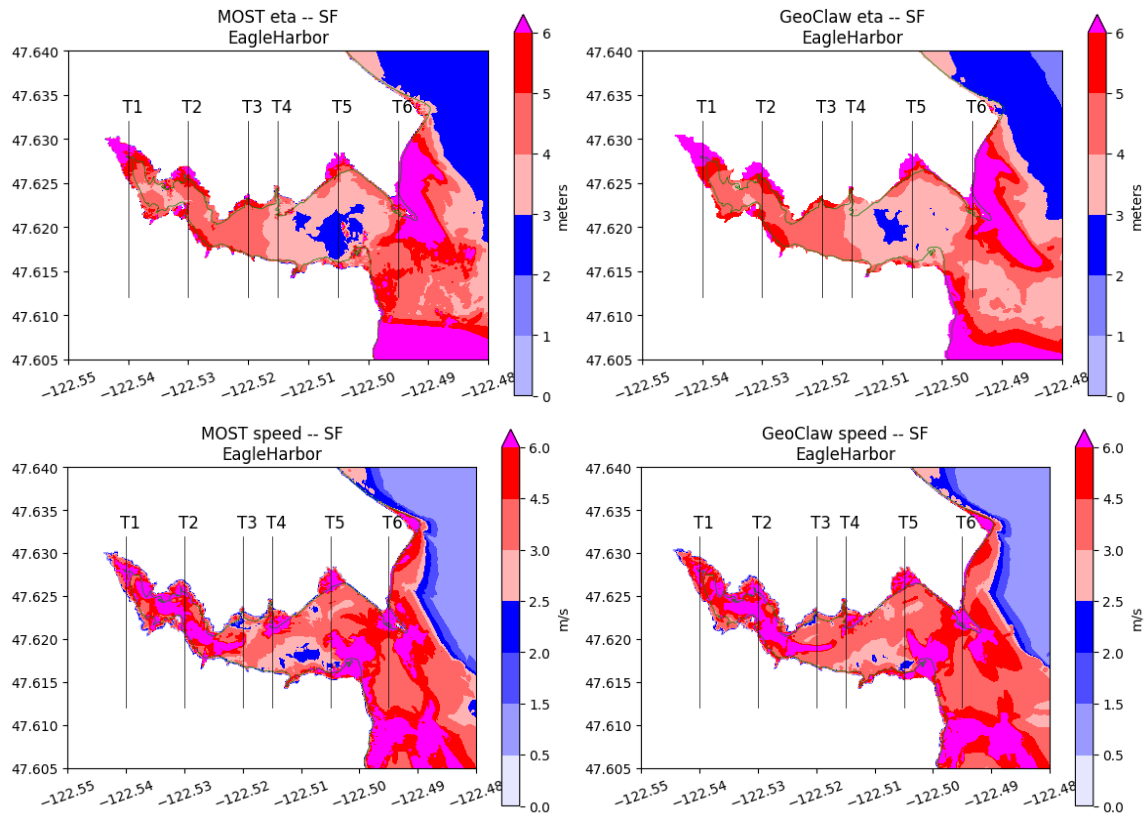


Figure 14: Comparison of MOST and GeoClaw results for the SF-L event in Eagle Harbor. Also shown is the location of transects. The following plots show cross sections of the maximum surface and speed along these transects.

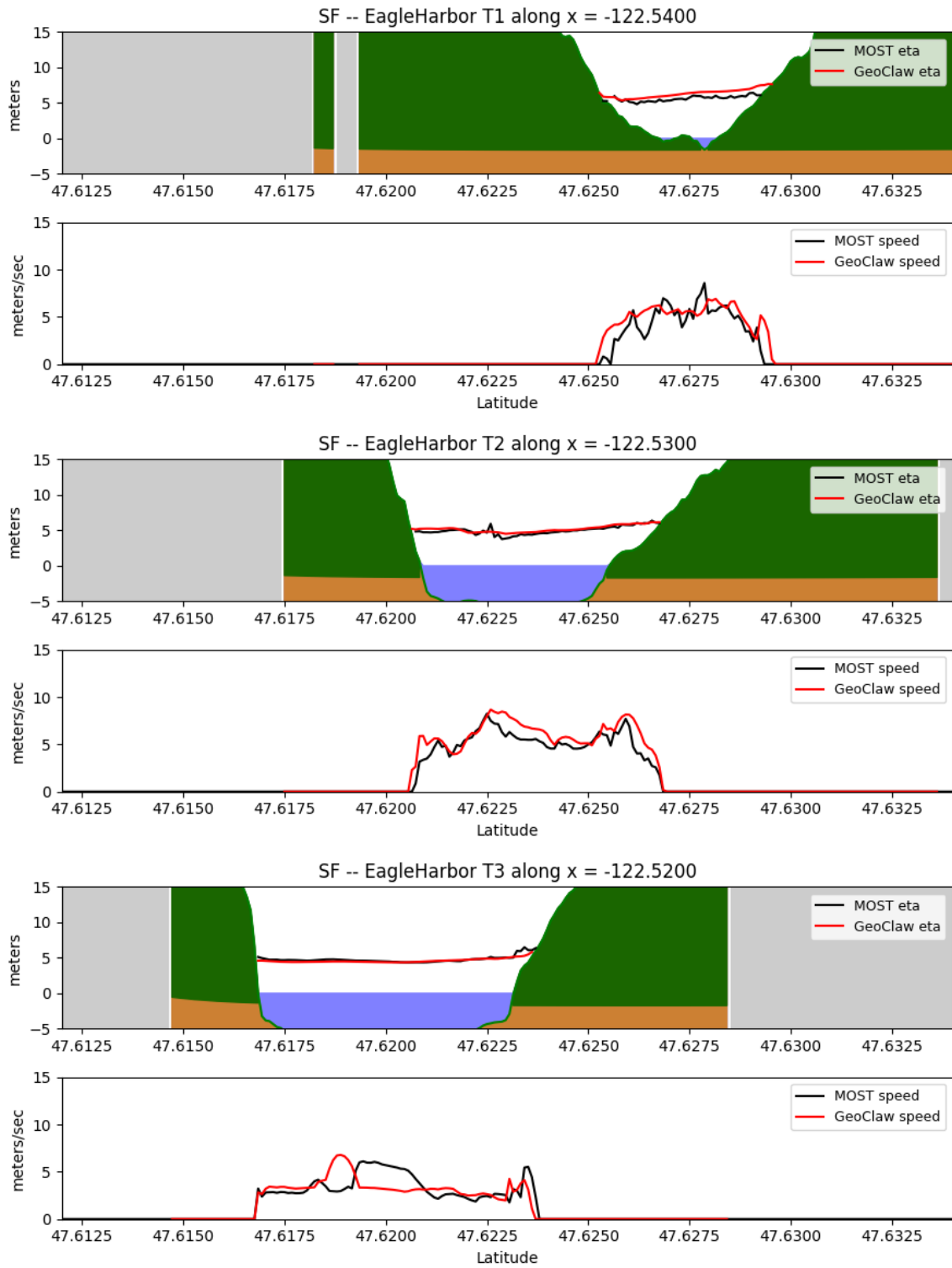


Figure 15: Comparison of MOST and GeoClaw results along Eagle Harbor transects T1–T3.

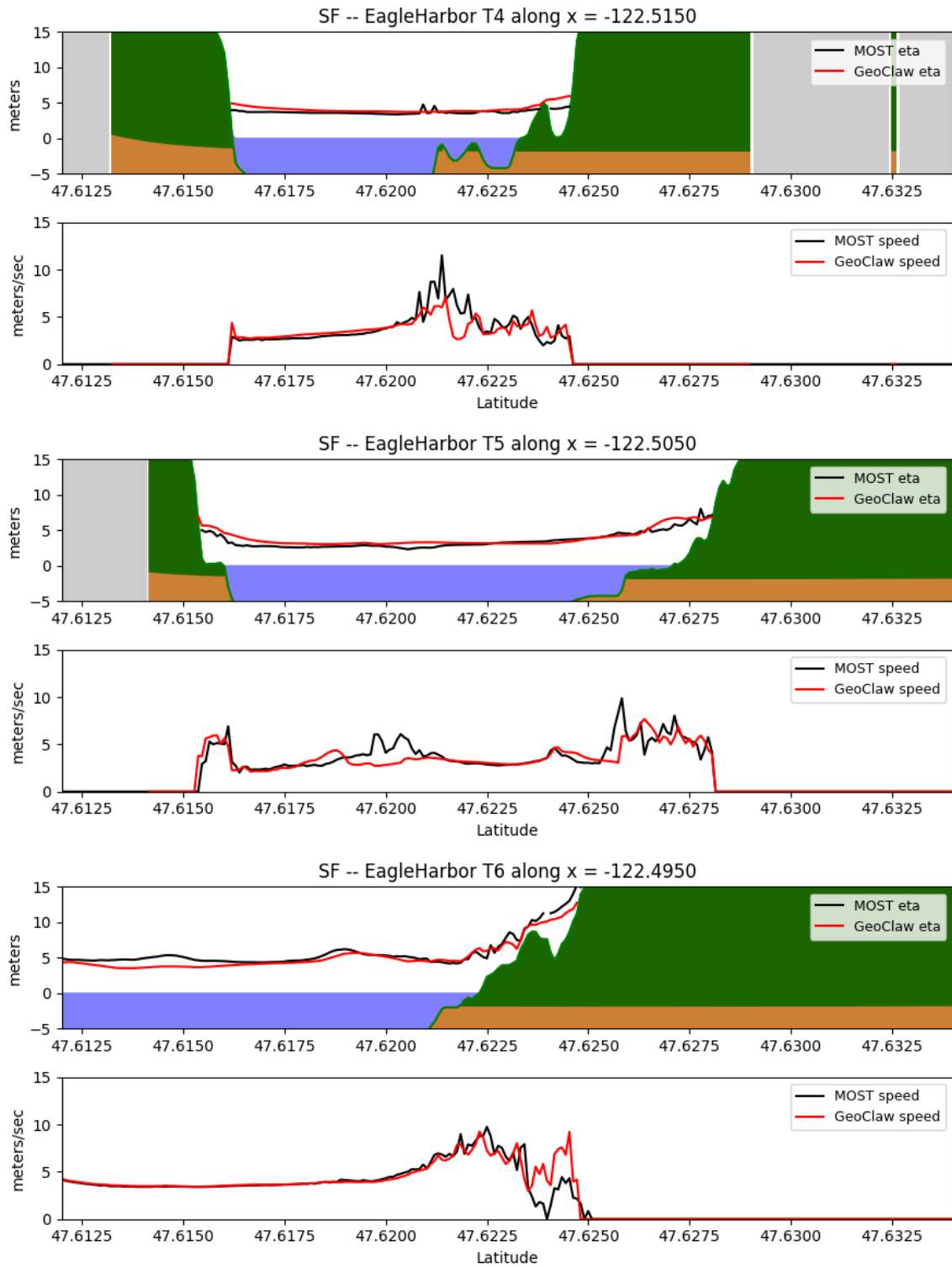


Figure 16: Comparison of MOST and GeoClaw results along Eagle Harbor transects T4–T6.

A.1.2 Seattle Fault SF-L, Murden Cove

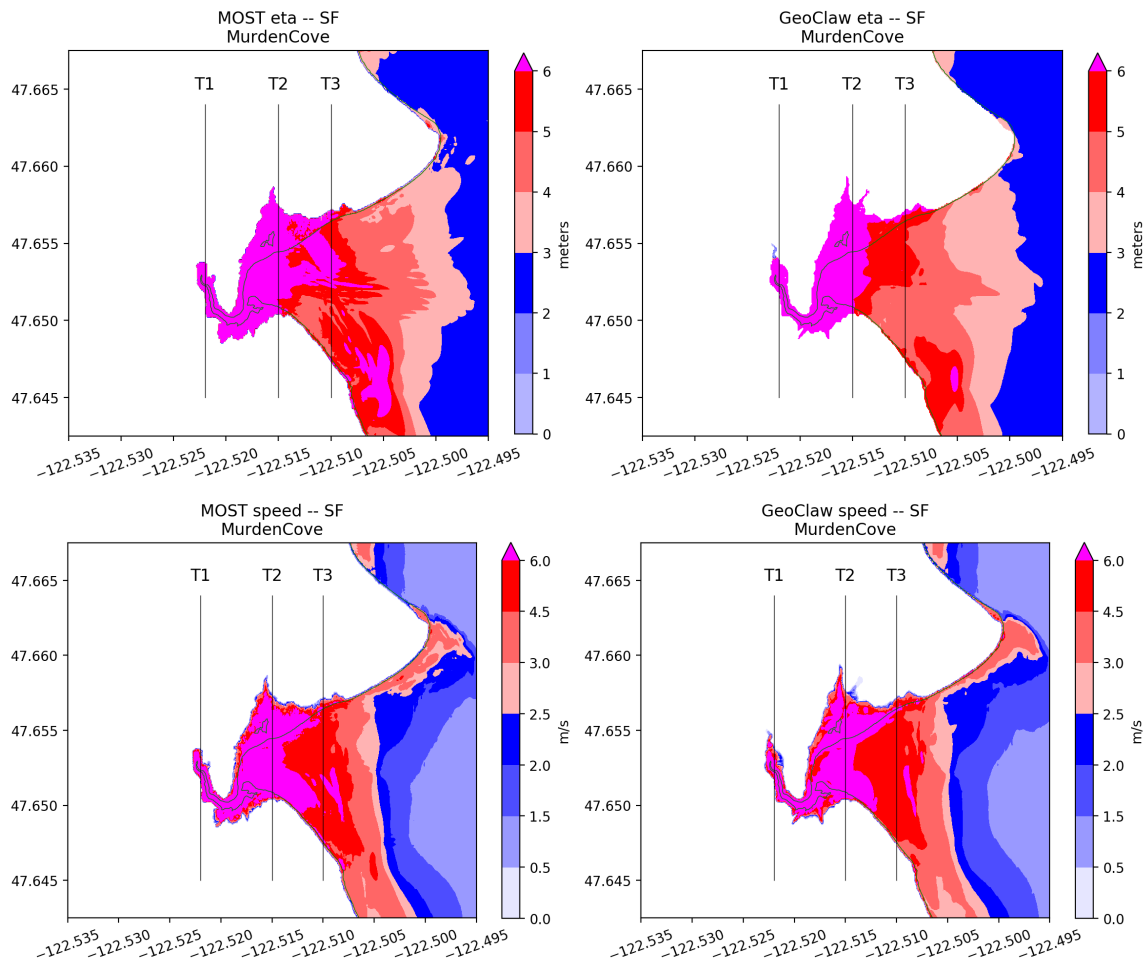


Figure 17: Comparison of MOST and GeoClaw results for the SF-L event in Murden Cove. Also shown is the location of transects. The following plots show cross sections of the maximum surface and speed along these transects.

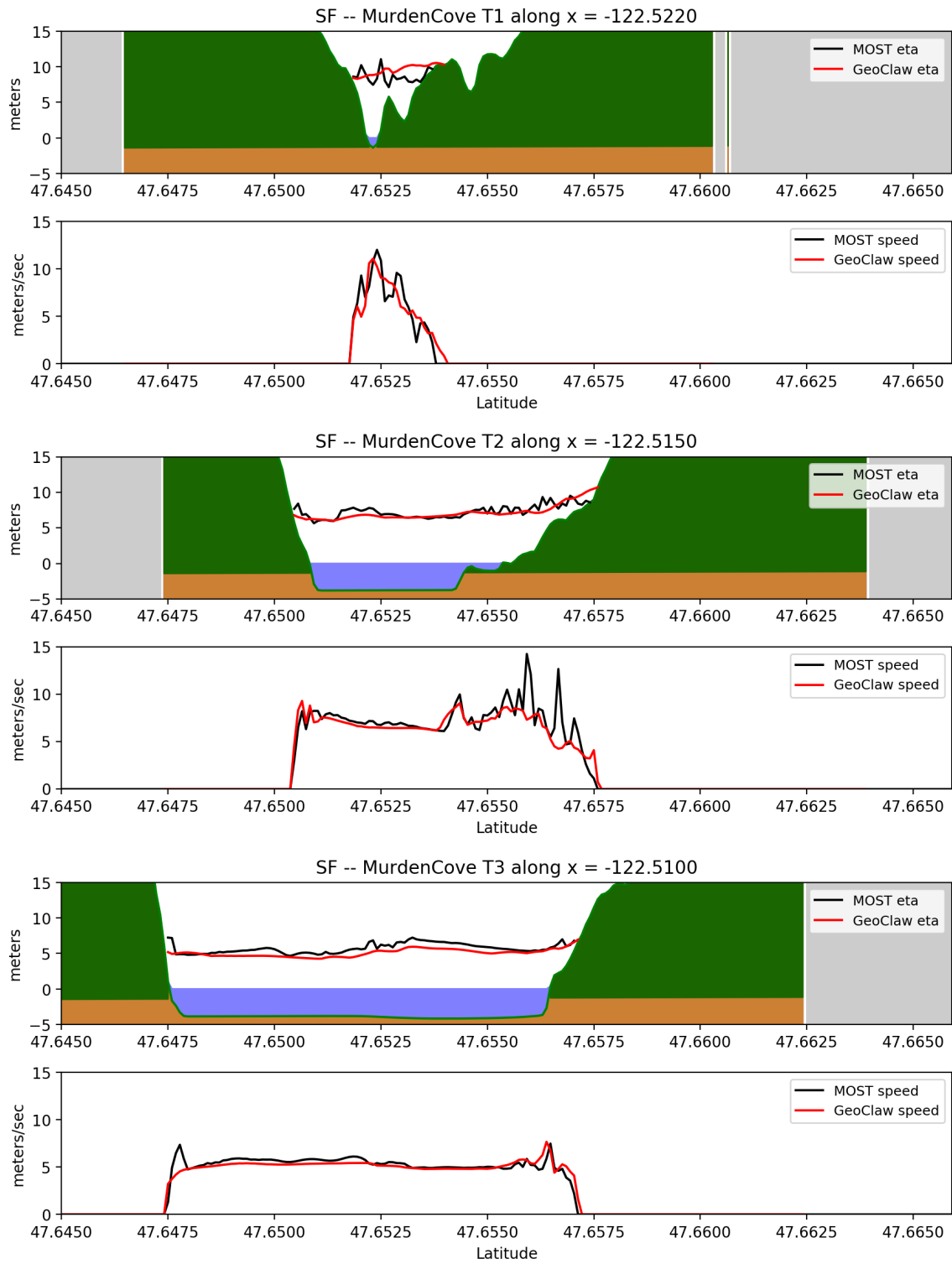


Figure 18: Comparison of MOST and GeoClaw results along Murden Cove transects.

A.1.3 Seattle Fault SF-L, Agate Pass

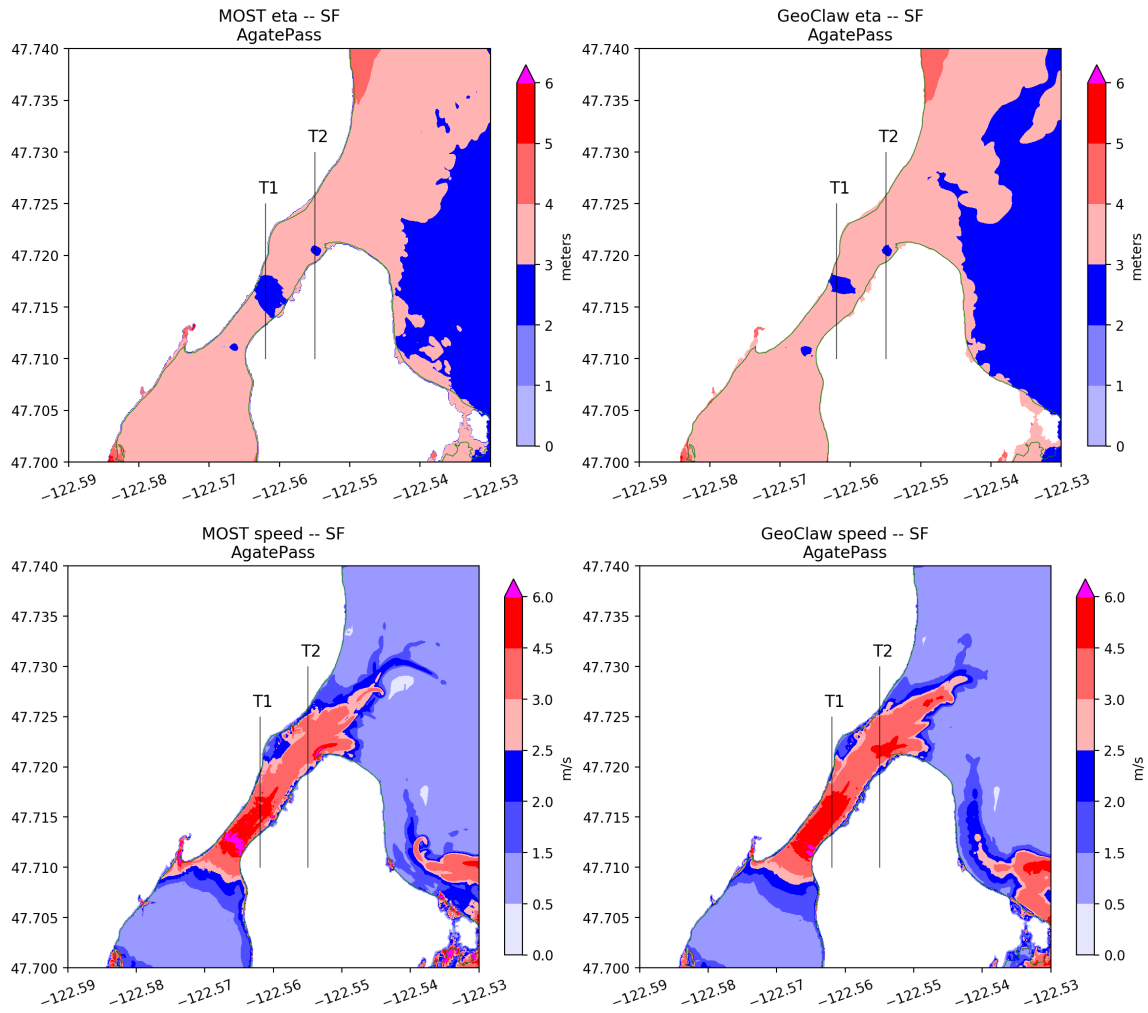


Figure 19: Comparison of MOST and GeoClaw results for the SF-L event around Agate Pass. Also shown is the location of transects. The following plots show cross sections of the maximum surface and speed along these transects.

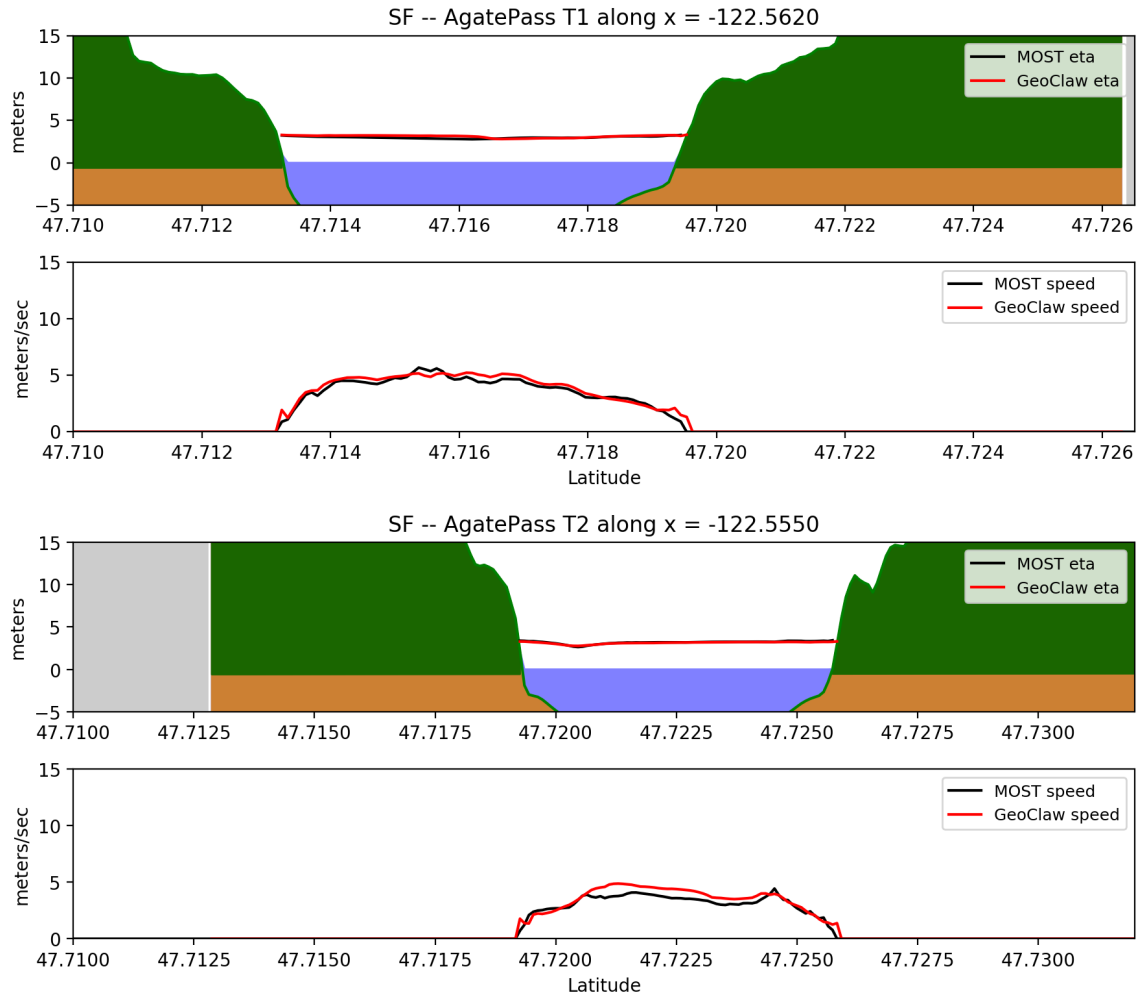


Figure 20: Comparison of MOST and GeoClaw results along Agate Pass transects.

A.1.4 Seattle Fault SF-L, Point White

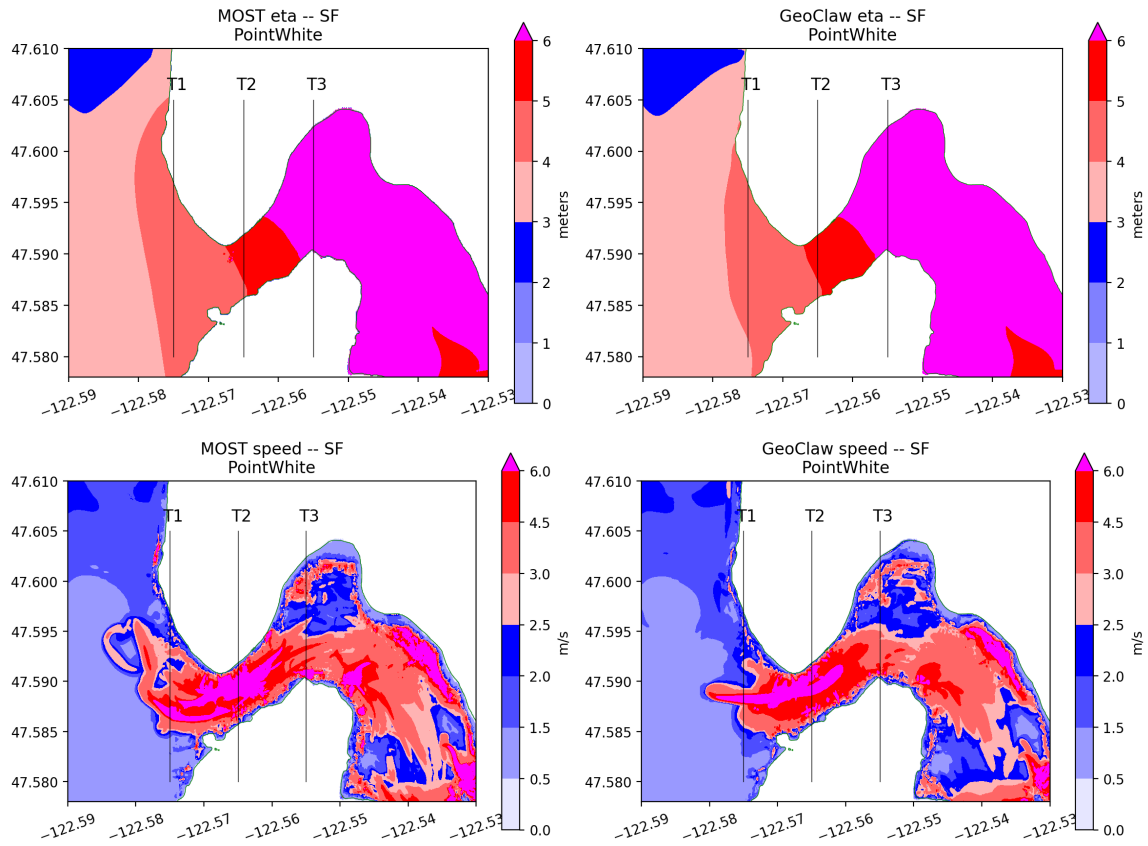


Figure 21: Comparison of MOST and GeoClaw results for the SF-L event around Point White. Also shown is the location of transects. The following plots show cross sections of the maximum surface and speed along these transects.

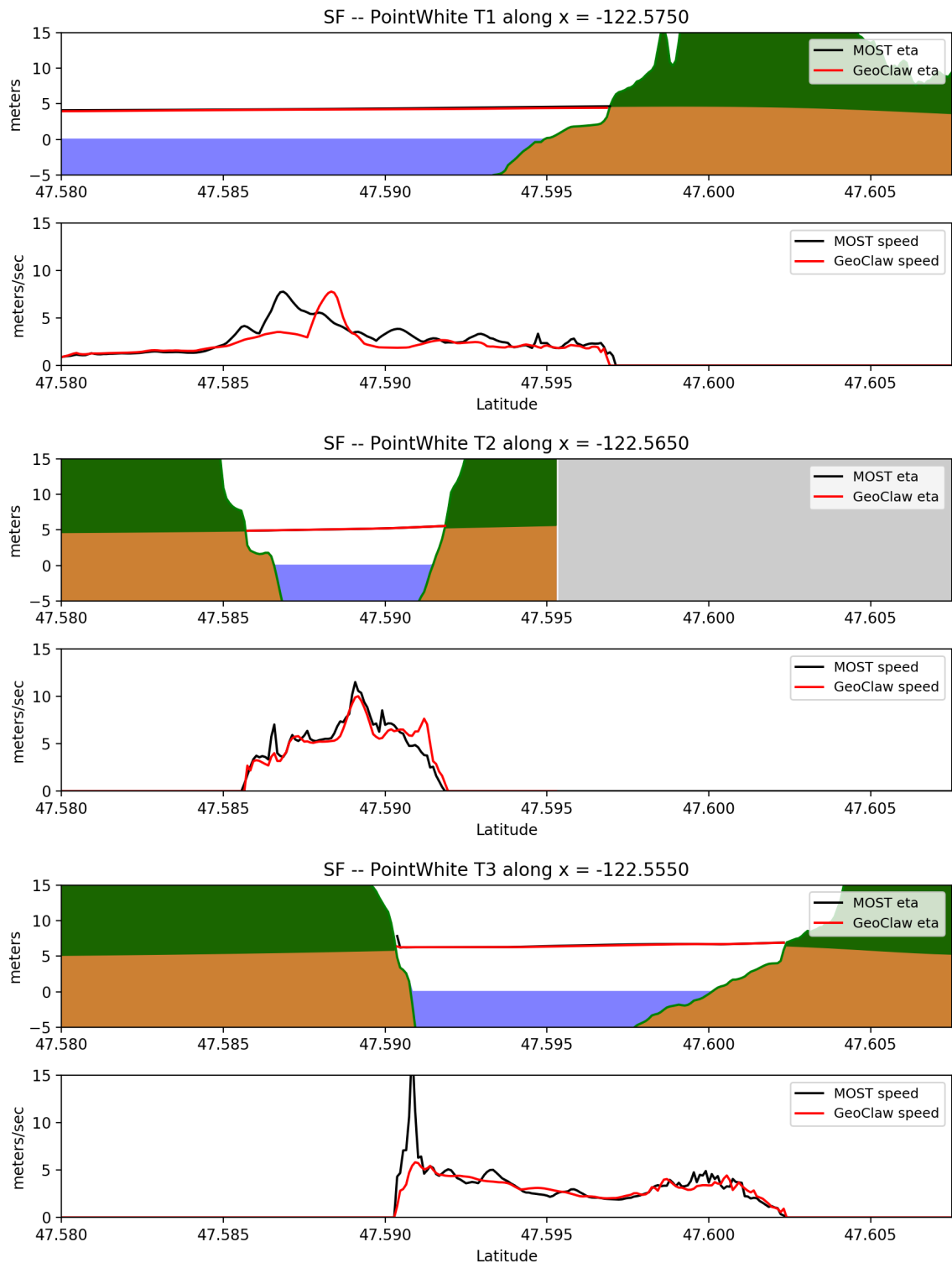


Figure 22: Comparison of MOST and GeoClaw results along Point White transects.

B Additional comparisons of results for CSZ L1

This appendix contains additional plots comparing the results obtained with MOST and those obtained with GeoClaw, for the CSZ event L1. Section [B.1](#) shows zoomed in views of the plots from [Figure 4](#) along with cross sections of the solution on a few transects. Section [8.2.2](#) shows time series results at several gauges.

B.1 Zoomed views and transect plots

The plots in the next sections first show a zoomed view of one portion of Bainbridge Island, with several transect locations indicated. Then the following plots show vertical slices along these transects. The format is the same as used for the SF-L results in [Section A.1](#); see the beginning of that section for more discussion of plots.

B.1.1 CSZ L1, Eagle Harbor

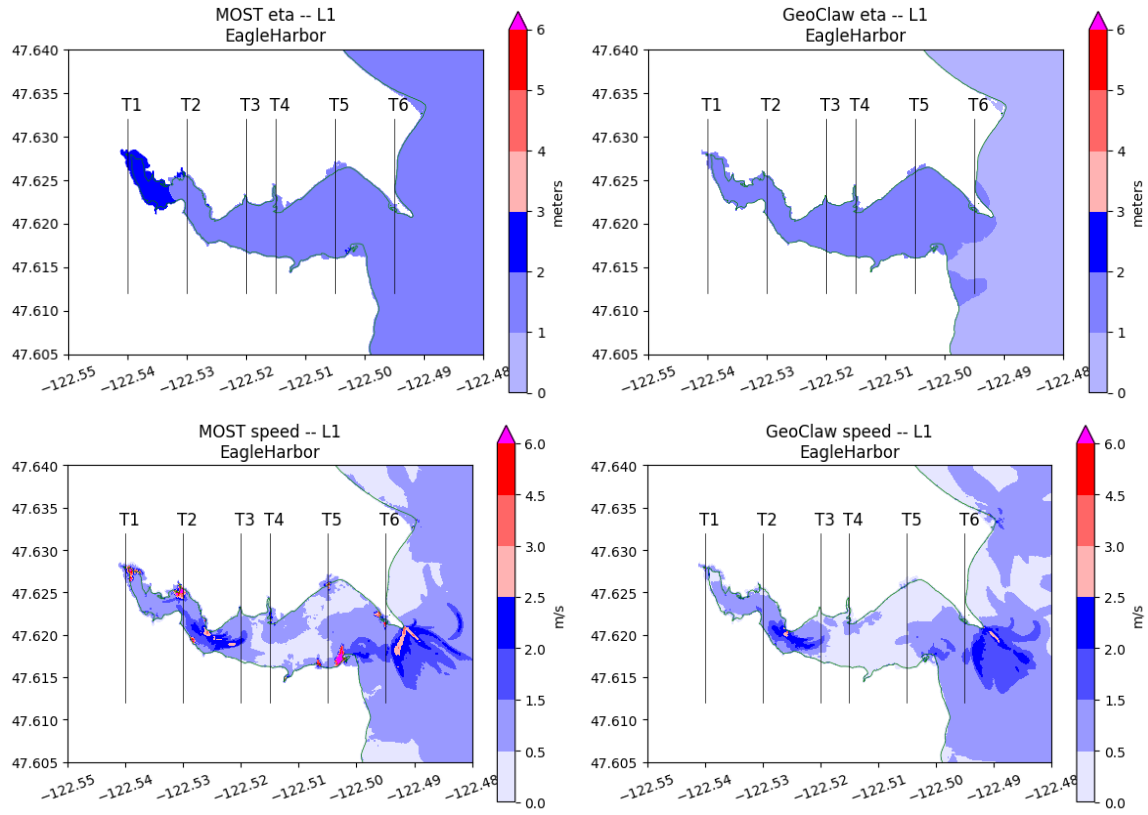


Figure 23: Comparison of MOST and GeoClaw results for the L1 event in Eagle Harbor. Also shown is the location of transects. The following plots show cross sections of the maximum surface and speed along these transects.

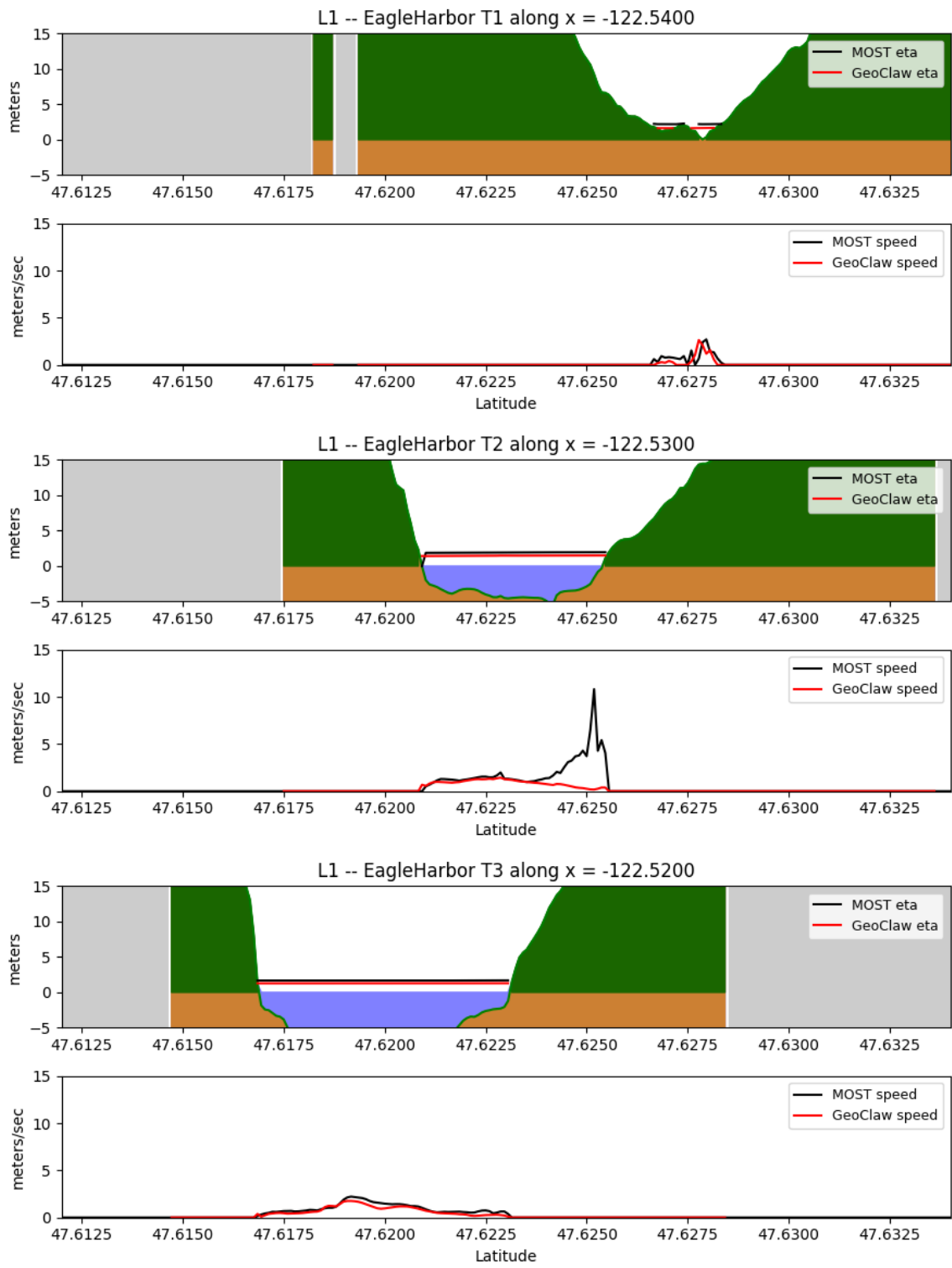


Figure 24: Comparison of MOST and GeoClaw results along Eagle Harbor transects.

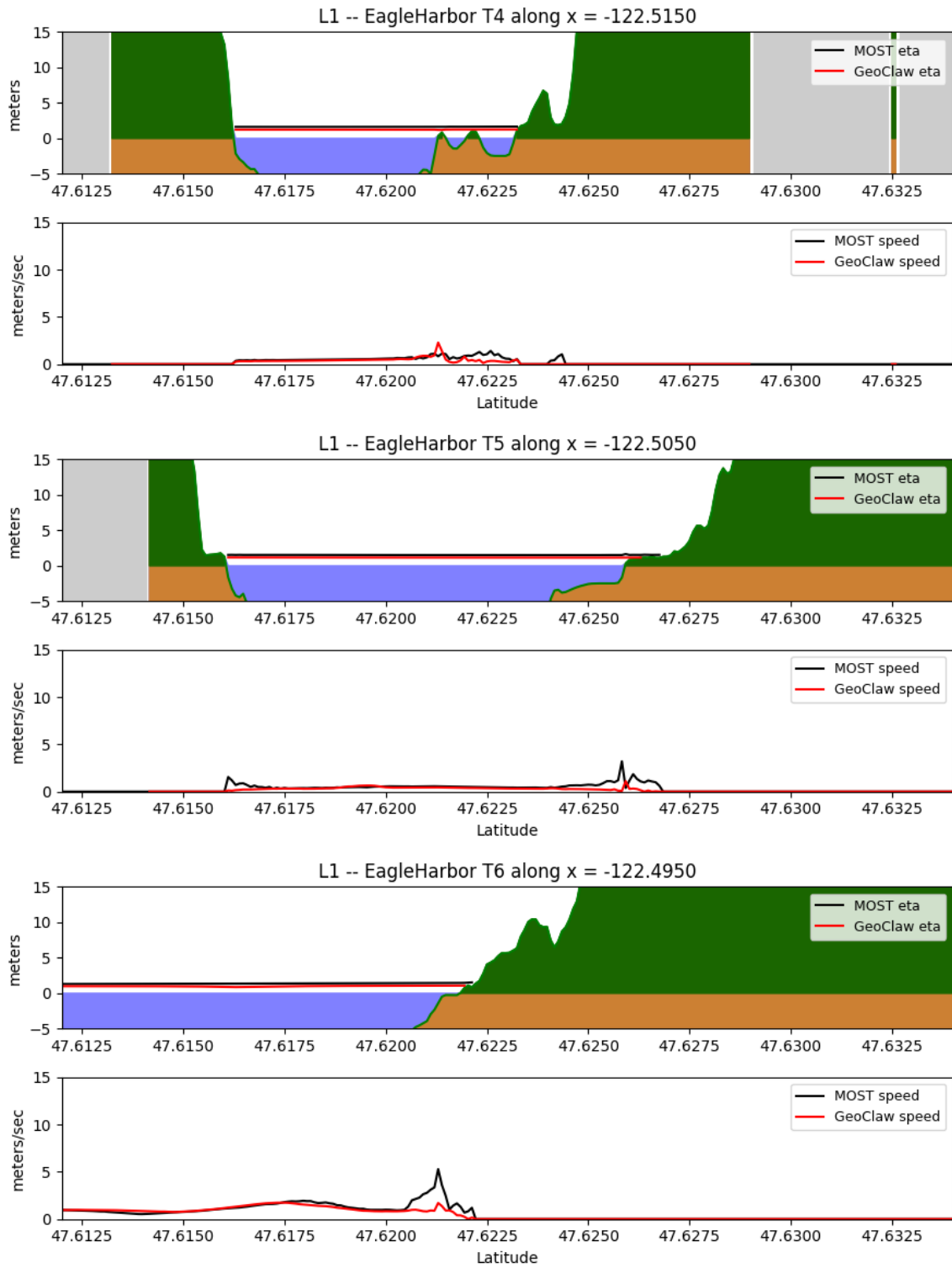


Figure 25: Comparison of MOST and GeoClaw results along Eagle Harbor transects.

B.1.2 CSZ L1, Murden Cove

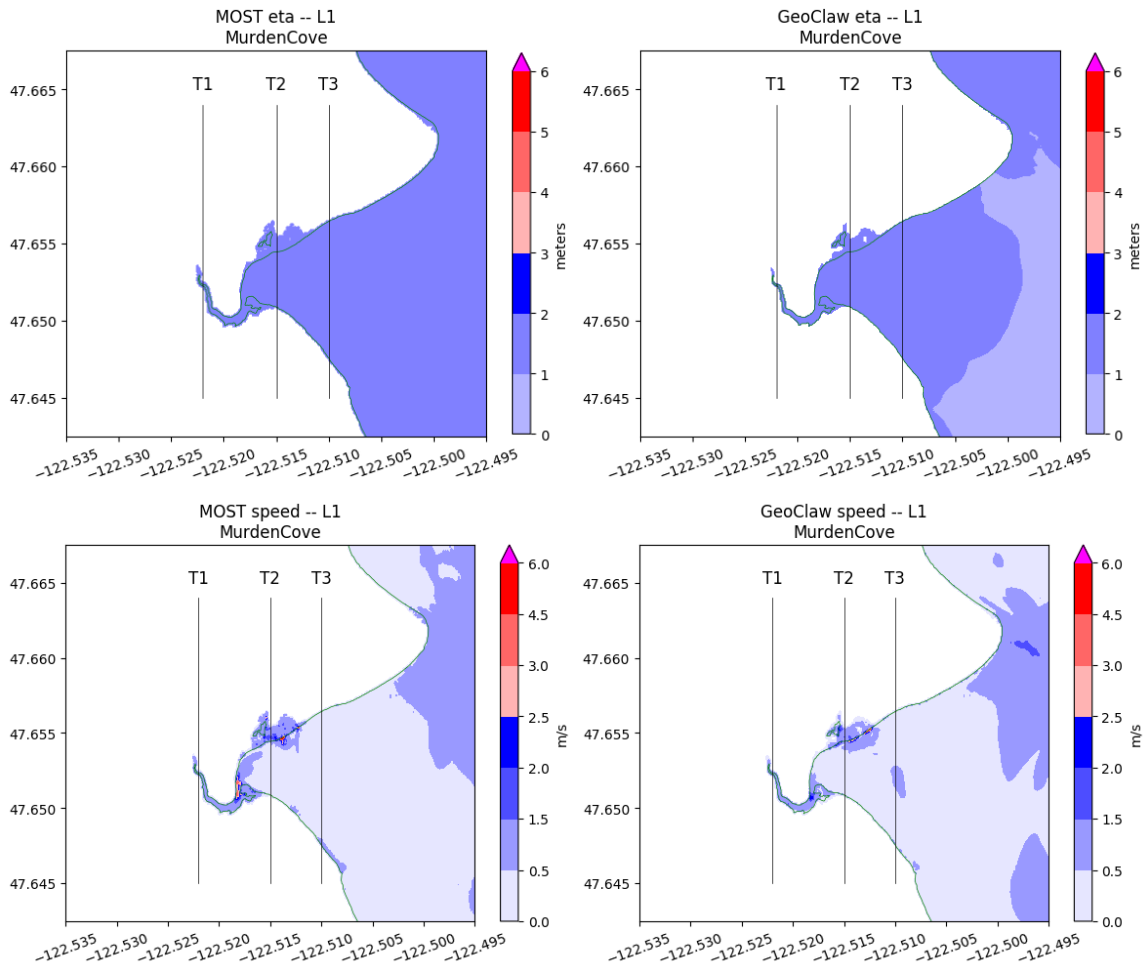


Figure 26: Comparison of MOST and GeoClaw results for the L1 event in Murden Cove. Also shown is the location of transects. The following plots show cross sections of the maximum surface and speed along these transects.

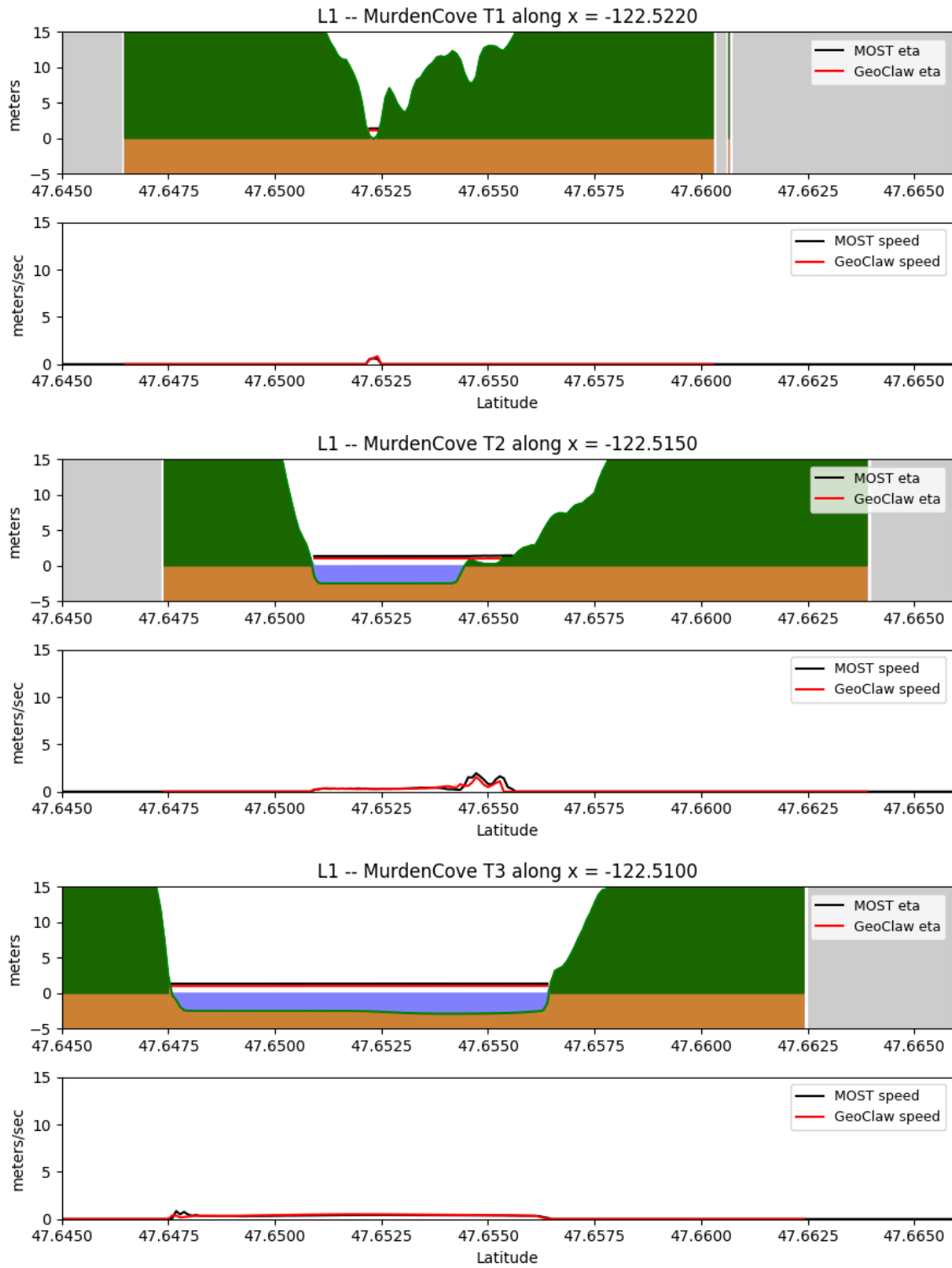


Figure 27: Comparison of MOST and GeoClaw results along Murden Cove transects.

B.1.3 CSZ L1, Agate Pass

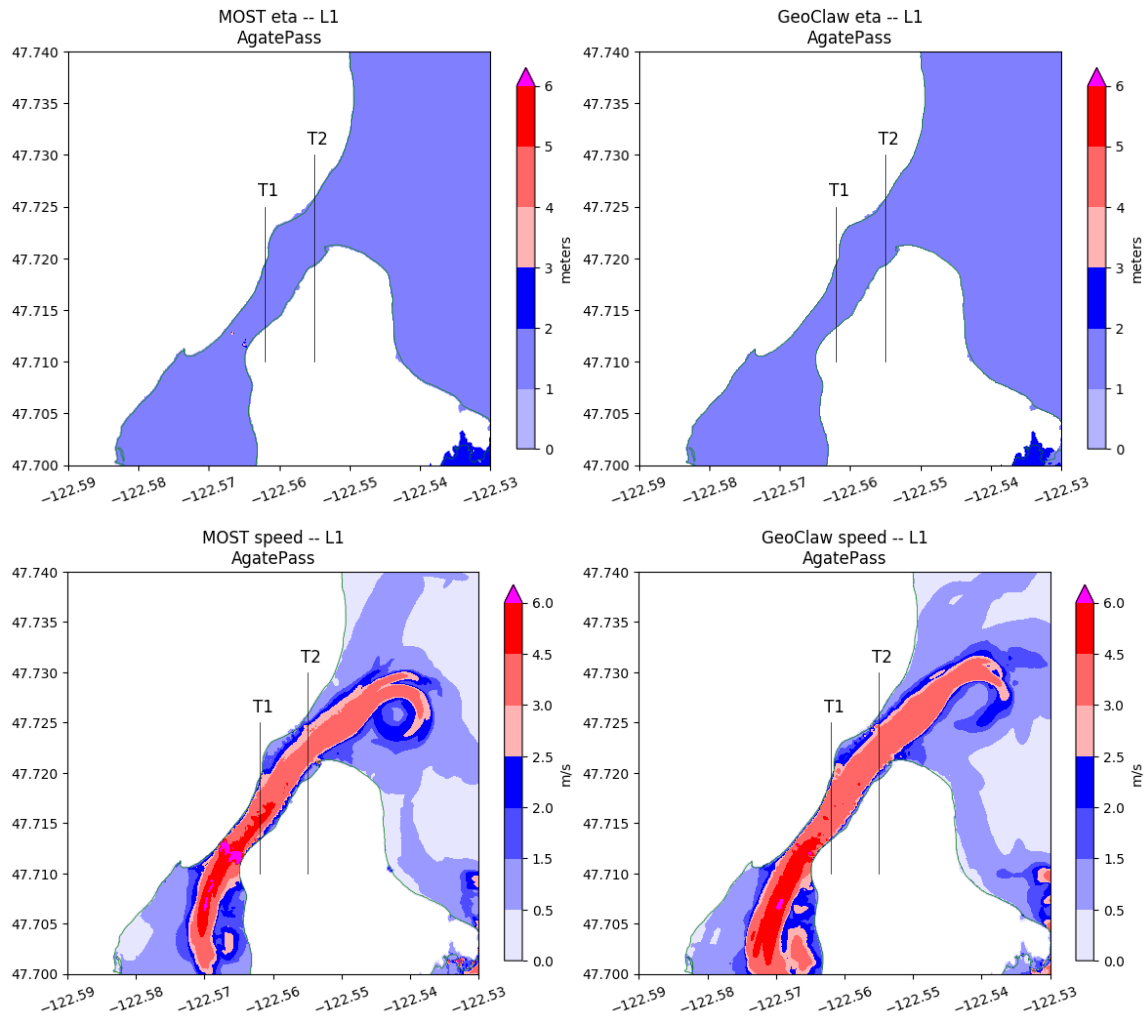


Figure 28: Comparison of MOST and GeoClaw results for the L1 event around Agate Pass. Also shown is the location of transects. The following plots show cross sections of the maximum surface and speed along these transects.

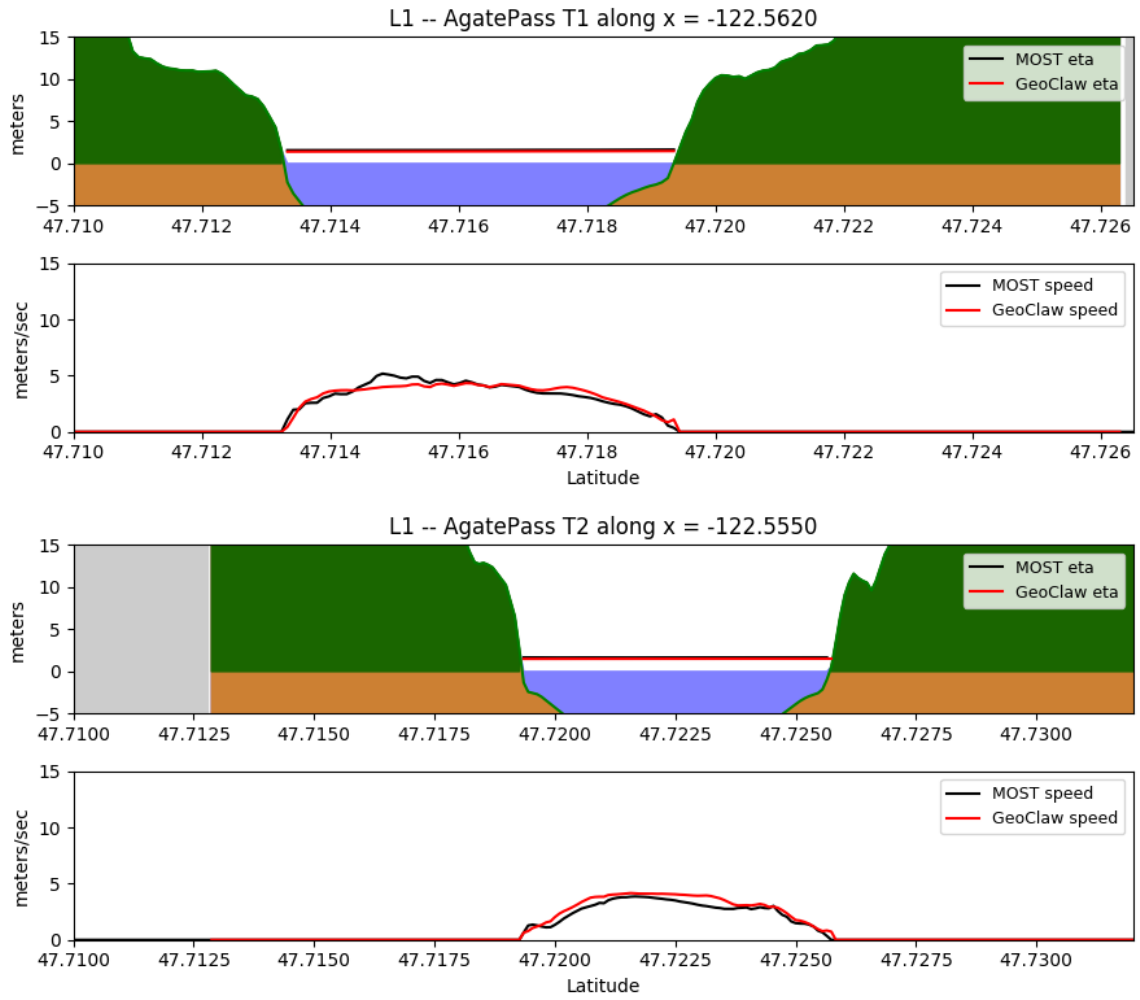


Figure 29: Comparison of MOST and GeoClaw results along Agate Pass transects.

B.1.4 CSZ L1, Point White

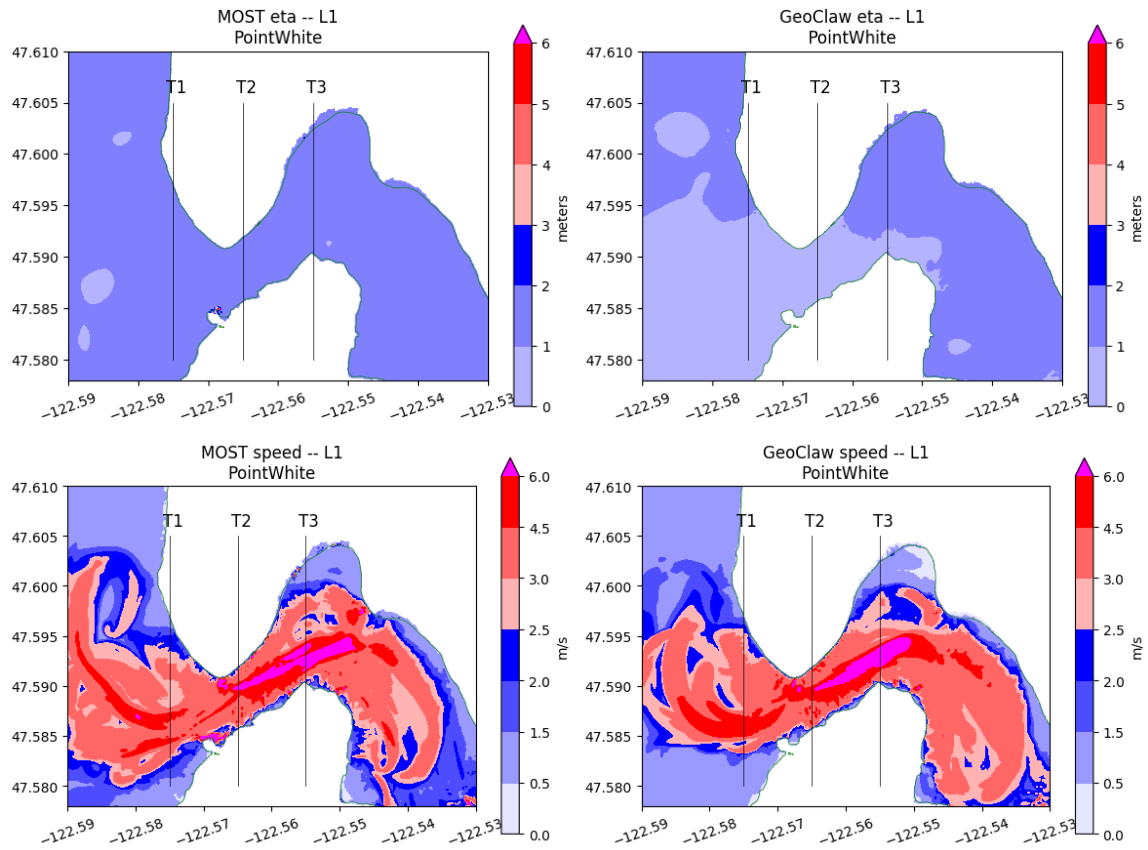


Figure 30: Comparison of MOST and GeoClaw results for the L1 event around Point White. Also shown is the location of transects. The following plots show cross sections of the maximum surface and speed along these transects.

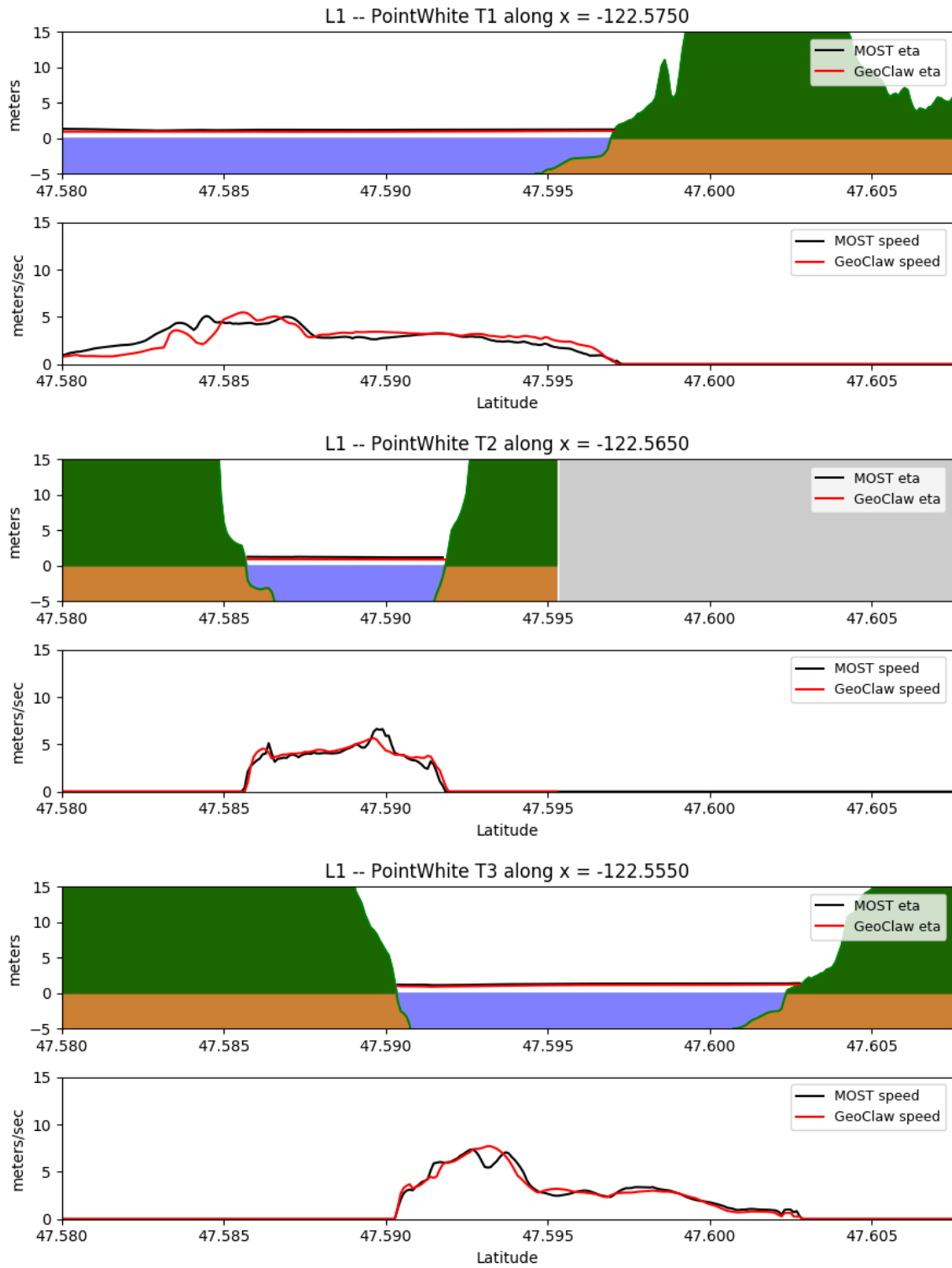


Figure 31: Comparison of MOST and GeoClaw results along Point White transects.

C GeoClaw Data format

For each earthquake source, output data is provided as csv files.

Format of fgmax output csv files.

The maximum depth, speed, and other quantities of interest over the full duration of the simulation is recorded in the csv files:

- `L1_bainbridge_fgmax.csv` results using the CSZ-L1 source,
- `SF_bainbridge_fgmax.csv` results using the Seattle Fault event SF-L.

Each file has a one-line header followed by a line of data for each fgmax point in the region. The columns are:

1. longitude (degrees)
2. latitude (degrees)
3. topography elevation z from the DEM (meters)
4. topography value B from GeoClaw for the grid cell (m)
5. subsidence dz interpolated from deformation file (m)
6. maximum fluid depth h (m)
7. maximum fluid velocity (m/s)
8. maximum momentum flux (m^3/s^2)
9. arrival time (seconds)

The fgmax points are exactly aligned with the $1/3''$ DEM, although sampled at $1/3''$ in longitude. The finest level computational finite volume grid is also aligned so that cell centers are exactly at the fgmax points, and z in column 3 is the value from the DEM at this point. However, the topography value B used in a grid cell in GeoClaw is obtained by integrating a piecewise bilinear function that interpolates the $1/3''$ DEM, and so B does not exactly equal z .

Format of gauge output csv files.

The gauge time series is recorded in csv files with columns

1. time (seconds post-quake),
2. topography value B from GeoClaw at gauge location (m),
3. depth of water at gauge in simulation (m),
4. E/W velocity u at gauge (m/s),
5. N/S velocity v at gauge (m/s).

Acknowledgments

The UW group acknowledges computing time provided by the CU-CSDMS High-Performance Computing Cluster, and by the Applied Mathematics Department at the University of Washington.

References

- [1] B. ATWATER, M.-R. SATOKO, K. SATAKE, T. YOSHINOBU, U. KAZUE, AND D. YAMAGUCHI. USGS professional paper 1707, 2005.
- [2] M. J. BERGER, D. L. GEORGE, R. J. LEVEQUE, AND K. T. MANDLI, *The geoclaw software for depth-averaged flows with adaptive refinement*. Preprint and simulations: www.clawpack.org/links/papers/awr10, 2010.
- [3] C. CHAMBERLAIN AND D. ARCAS, *Modeling tsunami inundation for hazard mapping at Everett, Washington, from the Seattle Fault*. OAA Technical Memorandum OAR PMEL-147, 2015, <https://doi.org/10.7289/V59Z92V0>, <https://repository.library.noaa.gov/view/noaa/11189>.
- [4] CLAWPACK DEVELOPMENT TEAM, *Clawpack software*, 2017, <https://doi.org/10.5281/zenodo.820730>, <http://www.clawpack.org>. Version 5.4.1.
- [5] F. GONZÁLEZ, R. J. LEVEQUE, J. VARKOVITZKY, P. CHAMBERLAIN, B. HIRAI, AND D. L. GEORGE, *Geo-Claw Results for the NTHMP Tsunami Benchmark Problems*. <http://depts.washington.edu/clawpack/links/nthmp-benchmarks/geoclaw-results.pdf>, 2011.
- [6] R. LEVEQUE, F. GONZÁLEZ, AND L. ADAMS, *Tsunami Hazard Assessment of Snohomish County, Washington, Project Report-Version 2*, 2018.
- [7] R. J. LEVEQUE, D. L. GEORGE, AND M. J. BERGER, *Tsunami modeling with adaptively refined finite volume methods*, *Acta Numerica*, (2011), pp. 211–289.
- [8] P. J. LYNETT, K. GATELY, R. WILSON, L. MONTOYA, ET AL., *Inter-model analysis of tsunami-induced coastal currents*, *Ocean Modelling*, 114 (2017), pp. 14–32, <https://doi.org/10.1016/j.ocemod.2017.04.003>, <http://www.sciencedirect.com/science/article/pii/S1463500317300513>.
- [9] M. D. PETERSEN, C. H. CRAMER, AND A. D. FRANKEL, *Simulations of Seismic Hazard for the Pacific Northwest of the United States from Earthquakes Associated with the Cascadia Subduction Zone*, *Pure Appl. Geophys.*, 159 (2002), pp. 2147–2168.
- [10] K. SATAKE, K. WANG, AND B. F. ATWATER, *Fault slip and seismic moment of the 1700 Cascadia earthquake inferred from Japanese tsunami descriptions*, *J. Geophys. Res.*, 108(B11) (2003), p. 2535, <https://doi.org/10.1029/2003JB002521>.
- [11] C. E. SYNOLAKIS, E. N. BERNARD, V. V. TITOV, U. KANOGLU, AND F. GONZÁLES, *Standards, criteria, and procedures for NOAA evaluation of tsunami numerical models*. NOAA Tech. Memo. OAR PMEL-135, 2007.
- [12] V. V. TITOV AND F. GONZALES, *Implementation and testing of the method of splitting tsunamis (MOST) model*. NOAA Tech. Memo. ERL PMEL-112, 1997.
- [13] V. V. TITOV, U. KANOGLU, AND C. SYNOLAKIS, *Development of most for real-time tsunami forecasting*, *J. Waterw. Port Coast. Ocean Eng.*, 142 (2016), p. 03116004, [https://doi.org/10.1061/\(ASCE\)WW.1943-5460.0000357](https://doi.org/10.1061/(ASCE)WW.1943-5460.0000357).
- [14] V. V. TITOV AND C. E. SYNOLAKIS, *Numerical modeling of tidal wave runup*, *Journal of Waterways, Ports, Coastal and Ocean Engineering*, 124 (1998), pp. 157–171.
- [15] R. C. WITTER, Y. ZHANG, K. WANG, G. PRIEST, C. GOLDFINGER, L. STIMELY, J. ENGLISH, AND P. FERRO, *Simulating tsunami inundation for a range of Cascadia megathrust earthquake scenarios at Bandon, Oregon USA*, *Geosphere*, 9 (2013), pp. 1783–1803.